

# Effective field theory for dilute Fermi systems at fourth order

C. Wellenhofer,<sup>1,2,\*</sup> C. Drischler,<sup>3,4,5,†</sup> and A. Schwenk<sup>1,2,6,‡</sup>

<sup>1</sup>*Technische Universität Darmstadt, Department of Physics, 64289 Darmstadt, Germany*

<sup>2</sup>*ExtreMe Matter Institute EMMI, GSI Helmholtzzentrum für Schwerionenforschung GmbH, 64291 Darmstadt, Germany*

<sup>3</sup>*Facility for Rare Isotope Beams, Michigan State University, MI 48824, United States of America*

<sup>4</sup>*Department of Physics, University of California, Berkeley, CA 94720, United States of America*

<sup>5</sup>*Nuclear Science Division, Lawrence Berkeley National Laboratory, Berkeley, CA 94720, United States of America*

<sup>6</sup>*Max-Planck-Institut für Kernphysik, Saupfercheckweg 1, 69117 Heidelberg, Germany*

We discuss high-order calculations in perturbative effective field theory for fermions at low energy scales. The Fermi-momentum or  $k_F a_s$  expansion for the ground-state energy of the dilute Fermi gas is calculated to fourth order, both in cutoff regularization and in dimensional regularization. For the case of spin one-half fermions we find from a Bayesian analysis that the expansion is well-converged at this order for  $|k_F a_s| \lesssim 0.5$ . Furthermore, we show that Padé-Borel resummations can improve the convergence for  $|k_F a_s| \lesssim 1$ . Our results provide important constraints for nonperturbative calculations of ultracold atoms and dilute neutron matter.

## I. INTRODUCTION

Over the last two decades, striking progress in quantum many-body physics has been achieved especially through well-controlled experiments with ultracold atoms and the development of efficient computational methods. Parallel to this, the conception of effective field theory (EFT) has equipped advanced many-body calculations with a firm theoretical basis. Here, we make a new contribution to these advances by providing analytic EFT results at high orders for a central problem of many-body theory and experiment: the ground-state energy of the dilute Fermi gas.

Effective field theory is deeply connected with the notion of universality [1], for which the dilute Fermi gas is a classic example. This universal many-body system describes both the physics of cold atomic gases as well as that of the dilute nuclear matter present in the crust of neutron stars. In ultracold-atom experiments, Feshbach resonances allow one to tune the interaction strength via the application of external fields. This makes it possible to probe low-density Fermi systems over a wide range of many-body dynamics, in particular at the unitary limit of infinite scattering length and through the BCS-BEC crossover [2–6]. Moreover, continuous progress with quantum Monte Carlo (QMC) methods [5, 7, 8] has enabled computations of strongly interacting dilute Fermi gases with a high precision comparable to that of experimental measurements. High-order analytic calculations that provide precision benchmarks for QMC and experiment represent an important tool for making further progress in this field. This is the focus of the present work.

Effective field theory provides the basis for such analytic benchmark calculations. In this context, the problem of renormalization, which historically has presented

a notable barrier for many-body calculations at high orders in perturbation theory, has been cleared up completely (in the perturbative case) [9–11]. While perturbative EFT calculations are generally restricted to low densities and weak interactions, respectively, they are still useful in many ways. Regarding the nuclear many-body problem [12–16], they provide viable input for constraining nuclear matter computations and neutron-star modeling. Via resummation methods, they also give access to approximate analytic results of large-scattering length physics.

Here, we present in detail the calculation and results to fourth order in the perturbative EFT for zero-temperature many-fermion systems at very low energies, i.e., the renowned Fermi-momentum or  $k_F a_s$  expansion for the ground-state energy of the dilute Fermi gas [17–27]. In that, we follow up on our recent Letter [28] where the first fourth-order results have been presented.<sup>1</sup> In the present paper, we expand substantially on the results and presentation of Ref. [28]. First, in Sec. II we discuss in more detail the contact EFT formalism for fermions at very low energy scales. In Sec. III we then present the details of the calculation of the Fermi-momentum expansion to fourth order for the case of spin one-half fermions. The case of spins greater than one-half is examined in detail in Sec. IV using two different regularization schemes: cutoff regularization and dimensional regularization. Our fourth-order results for the ground-state energy of the general dilute Fermi gas are then summarized in Sec. V. Using Bayesian methods, in Sec. VI we investigate the convergence of the Fermi-momentum expansion. There, we also study various Padé and Borel approximants constructed from the expansion. Finally, Sec. VII provides a short summary.

\* E-mail: [wellenhofer@theorie.ikp.physik.tu-darmstadt.de](mailto:wellenhofer@theorie.ikp.physik.tu-darmstadt.de)

† E-mail: [drischler@frib.msu.edu](mailto:drischler@frib.msu.edu)

‡ E-mail: [schwenk@physik.tu-darmstadt.de](mailto:schwenk@physik.tu-darmstadt.de)

<sup>1</sup> We note the following typos in Ref. [28]: in Eq. (21) and (25) a factor  $M^3$  is missing, and below Eq. (24) it should read II6(ii) instead of III6(ii).

## II. EFFECTIVE FIELD THEORY FOR NONRELATIVISTIC FERMIONS

The effective field theory (EFT) Lagrangian  $\mathcal{L}_{\text{EFT}}$  for dilute Fermi systems is composed of the most general two- and many-body contact interactions consistent with Galilean invariance, parity, and time-reversal invariance. Up to field redefinitions, its leading terms are given by (see, e.g., Refs. [11, 29–33])

$$\begin{aligned} \mathcal{L}_{\text{EFT}} = & \psi^\dagger \left[ i\partial_t + \frac{\vec{\nabla}^2}{2M} \right] \psi - \frac{C_0}{2} (\psi^\dagger \psi)^2 \\ & + \frac{C_2}{16} \left[ (\psi\psi)^\dagger (\psi \vec{\nabla}^2 \psi) + \text{H.c.} \right] \\ & + \frac{C'_2}{8} (\psi \vec{\nabla} \psi)^\dagger \cdot (\psi \vec{\nabla} \psi) - \frac{D_0}{6} (\psi^\dagger \psi)^3 + \dots, \end{aligned} \quad (1)$$

where  $\psi$  are nonrelativistic fermion fields,  $\vec{\nabla} = \vec{\nabla} - \vec{\nabla}$  is the Galilean invariant derivative, H.c. is the Hermitian conjugate, and  $M$  is the fermion mass. The couplings of the contact interactions  $C_0, C_2, C'_2, D_0, \dots$ , called low-energy constants (LECs), have to be fit to experimental data or (if possible) matched to an underlying theory. (For recent work aimed at rooting contact EFT for nucleons in lattice QCD calculations, see Refs. [34, 35].)

A truncation scheme, known as power counting, is required to organize the (infinite number of) EFT operators in a systematic way. In particular, the power counting needs to renormalize the ultraviolet (UV) divergences at each order. For perturbative calculations within the contact EFT given by Eq. (1), the power counting corresponds to ordering contributions in perturbation theory according to the (naive) mass dimension  $\sigma$  of the LECs, i.e.,

$$\sigma(C_{2n}^{(l)}) = 2n + 1, \quad (2)$$

$$\sigma(D_{2n}^{(l)}) = 2n + 4, \quad (3)$$

$$\sigma(E_{2n}^{(l)}) = 2n + 7, \quad (4)$$

etc., where the LECs  $E_{2n}^{(l)}$  correspond to four-body interactions.

In the following, we first discuss in Sec. II A the relation between  $N$ -body scattering diagrams and the MBPT series for dilute Fermi systems. This is followed by the analysis of UV power divergences and two-body scattering diagrams in Sec. II B. In Sec. II C we then examine the ladder diagrams of MBPT. Next, in Sec. II D we study the renormalization of logarithmic UV divergences and the associated nonanalytic terms in the perturbative EFT expansion. Finally, Sec. II E briefly discusses different partial resummations for systems with a large  $S$ -wave scattering length.

### A. Renormalization from few-body to many-body systems

The nonrelativistic field theory specified by the Lagrangian  $\mathcal{L}_{\text{EFT}}$  is equivalent to a Hamiltonian approach with  $N$ -body potentials. The regularized two- and three-body potentials are given by

$$\begin{aligned} \langle \mathbf{p}' | V_{\text{EFT}}^{(2)} | \mathbf{p} \rangle = & \left[ C_0(\Lambda) + C_2(\Lambda)(\mathbf{p}'^2 + \mathbf{p}^2)/2 \right. \\ & \left. + C'_2(\Lambda) \mathbf{p}' \cdot \mathbf{p} + \dots \right] f(p/\Lambda) f(p'/\Lambda), \end{aligned} \quad (5)$$

$$\begin{aligned} \langle \mathbf{p}' \mathbf{q}' | V_{\text{EFT}}^{(3)} | \mathbf{p} \mathbf{q} \rangle = & \left[ D_0(\Lambda) + \dots \right] f(p/\Lambda) f(q/\Lambda) \\ & \times f(p'/\Lambda) f(q'/\Lambda). \end{aligned} \quad (6)$$

Here,  $\mathbf{p}^{(l)}$  and  $\mathbf{q}^{(l)}$  are relative and Jacobi momenta, respectively, and  $f(p/\Lambda)$  is a regulator function that suppresses high-momentum modes. Later we will also consider dimensional regularization (DR), but for now we use a (Galilean invariant) momentum regulator.

The superficial degree of divergence  $d$  of an  $N$ -body scattering diagram is given by

$$d = 5L - 2I + \sum_{j=1}^{\mathcal{V}} [\sigma(g_j) - 1], \quad (7)$$

where  $L$  is the loop number,  $I$  the number of internal lines,  $\mathcal{V}$  the number of vertices, and  $g_j \in \{C_{2n}, D_{2n}, \dots\}$ ; see, e.g., Refs. [36, 37] for details. [If there are subdivergences the actual degree of divergence can be larger than  $d$ .] The MBPT diagrams are obtained from scattering diagrams by closing the external lines (and excluding occupied states in loop integrals) of a single scattering diagram, or by closing and connecting the external lines of several diagrams. Since the hole propagators associated with closed external lines are bounded (or exponentially decaying at finite temperature), the renormalization of MBPT follows from the renormalization of scattering diagrams. For nonrelativistic contact interactions,  $N$ -body scattering diagrams can have only up to  $N$  intermediate lines between adjacent vertices, so only  $N'$ -body interactions with  $N' \leq N$  appear in a given the  $N$ -body sector. This implies that the renormalization of the EFT interactions can be set up hierarchically, starting from the renormalization of two-body interactions in the two-body sector, then three-body, and so on, up to a given truncation order in the power counting.

### B. Two-body scattering

In the nonrelativistic EFT, the only two-body scattering diagrams are ladder diagrams (corresponding to iterations of the Lippmann-Schwinger equation), see Fig. 1. This makes the two-body sector very simple: all loop

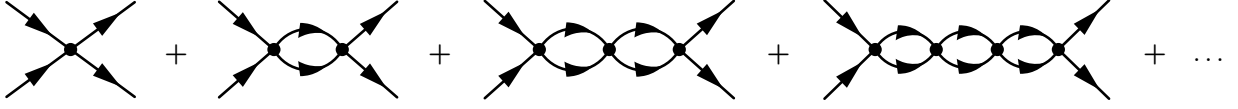


Figure 1. The two-body scattering diagrams. By closing the external lines one obtains the particle-particle ladder diagrams of MBPT. The momentum integration associated with the closed lines has the effect that the (MBPT) ladder series has zero radius of convergence (renormalon divergence), in contrast to the series of two-body scattering diagrams (a geometric series). See the text for details.

integrals factorize, with factors  $J_n(k, \Lambda)$  given by

$$J_n(k, \Lambda) = \int_0^\infty dq \frac{q^{2n}}{k^2 - q^2 + i\epsilon} f^2(q/\Lambda). \quad (8)$$

To extract the power divergence we rescale the loop momentum as  $\mathbf{q} \rightarrow \mathbf{q}/\Lambda$ , leading to

$$J_n(k, \Lambda) = I_n^{\text{UV}}(k, \Lambda) + J_n^R(k), \quad (9)$$

where

$$J_n^R(k) = \frac{i\pi}{2} k^{2n+1} \quad (10)$$

and  $I_n^{\text{UV}}(k, \Lambda) = I_n^{\text{UV},\infty}(k, \Lambda) + I_n^{\text{UV},0}(k, \Lambda)$ , with

$$I_n^{\text{UV},\infty}(k, \Lambda) = - \sum_{m=0}^n \alpha_{2m} \Lambda^{2m+1} k^{2(n-m)}, \quad (11)$$

$$I_n^{\text{UV},0}(k, \Lambda) \xrightarrow{\Lambda \rightarrow \infty} 0, \quad (12)$$

where  $\alpha_{2m}$  are regulator-dependent constants. The effective-range expansion (ERE) for the on-shell  $T$  matrix reads [11, 38]

$$T(k, \cos \vartheta) = \frac{4\pi}{M} \left\{ \underbrace{\sum_{n=0}^{\infty} \tau_n^{(s)} k^n}_{T^{(s)}(k)} + \underbrace{\sum_{n=2}^{\infty} \tau_n^{(p)} [k \cos \vartheta]^n}_{T^{(p)}(k, \cos \vartheta)} + \dots \right\}, \quad (13)$$

where  $k$  and  $\vartheta$  are the scattering momentum and angle, and

$$\tau_n^{(s)} = \{a_s, -ia_s^2, -a_s^3 + a_s^2 r_s, i(a_s^4 - 2a_s^3 r_s), a_s^5 - 3a_s^4 r_s + a_s^3 r_s^2 + a_s^2 v_s, \dots\}, \quad (14)$$

$$\tau_n^{(p)} = \{a_p^3, \dots\}, \quad (15)$$

with  $a_s$  and  $a_p$  the  $S$ - and  $P$ -wave scattering length, respectively,  $r_s$  the  $S$ -wave effective range, and  $v_s$  the  $S$ -wave shape parameter. Matching the regularized EFT perturbation series to Eq. (13) leads (in the infinite-cutoff limit  $\Lambda \rightarrow \infty$ ) to

$$C_0(\Lambda) = C_0 + C_0 \sum_{\nu=1}^3 \left( \alpha_0 C_0 \frac{M}{2\pi^2} \Lambda \right)^\nu + \alpha_2 C_2 C_0 \frac{M}{3\pi^2} \Lambda^3 + \dots, \quad (16)$$

$$C_2(\Lambda) = C_2 + \alpha_2 C_2 C_0 \frac{M}{\pi^2} \Lambda + \dots, \quad (17)$$

$$C'_2(\Lambda) = C'_2 + \dots, \quad (18)$$

where the cutoff-dependent parts are counterterms that cancel UV divergences and the omitted terms correspond to counterterms beyond fourth order. Note that all the counterterms required to renormalize  $C_0$ -only contributions to the  $T$  matrix are included in  $C_0(\Lambda)$ ; i.e., the  $C_0$  term corresponds to a perturbatively renormalizable interaction. For spin multiplicities  $g > 2$ , this feature is however restricted to the two-body sector (see Sec. IID).

The (renormalized) LECs are given by

$$C_0 = \frac{4\pi a_s}{M}, \quad C_2 = C_0 \frac{a_s r_s}{2}, \quad C'_2 = \frac{4\pi a_p^3}{M}, \quad (19)$$

etc. The perturbative EFT expansion is viable throughout the energy range appropriate to the EFT only if the size of the LECs conforms to the power counting; i.e.,

$$C_0 \sim \frac{1}{M\Lambda_b}, \quad C_2 \sim C'_2 \sim \frac{1}{M\Lambda_b^3}, \quad (20)$$

etc., corresponding to  $a_s \sim r_s \sim a_p \sim 1/\Lambda_b$ . Here,  $\Lambda_b$  is the ‘‘hard scale’’ beyond which the EFT description breaks down. The scaling given by Eq. (20) is commonly referred to as the ‘‘natural’’ case [38]. The EFT perturbation series then corresponds to an expansion in powers of  $Q/\Lambda_b$ .

### C. Many-body ladder diagrams and renormalons

Closing the external lines of two-body scattering diagrams, one obtains the particle-particle ( $pp$ ) ladder diagrams of MBPT. For these diagrams, the factors corresponding to the  $pp$  bubbles are given by

$$\mathcal{J}_n(P, k, \Lambda) = \int \frac{d^3q}{4\pi} \frac{q^{2n}}{k^2 - q^2} \bar{n}_{|\mathbf{P}-\mathbf{q}|/2} \bar{n}_{|\mathbf{P}+\mathbf{q}|/2} f^2(q/\Lambda), \quad (21)$$

where  $\bar{n}_k = \theta(k - k_F)$ ,  $k_F$  is the Fermi momentum, and  $\mathbf{q}$  is the relative momentum of the two particle lines in a given  $pp$  bubble. The hole lines correspond to integrating over  $\mathbf{P}$  and  $\mathbf{k}$ . The  $pp$  bubble can be separated as

$$\mathcal{J}_n(P, k) = I_n^{\text{UV}}(k, \Lambda) + \mathcal{J}_n^R(P, k), \quad (22)$$

where the cutoff-independent part is given by

$$\begin{aligned} \mathcal{J}_n^R(P, k) &= \int \frac{d^3q}{4\pi} \frac{q^{2n}}{k^2 - q^2} [\bar{n}_{|\mathbf{P}-\mathbf{q}|/2} \bar{n}_{|\mathbf{P}+\mathbf{q}|/2} - 1] \\ &= \frac{k_F}{2} + \frac{P}{2} + \frac{k}{2} \ln \left| \frac{k_F + P - k}{k_F + P + k} \right| \\ &\quad + \frac{k_F^2 - P^2 - k^2}{4P} \ln \left| \frac{(k_F + P)^2 - k^2}{k_F^2 - P^2 - k^2} \right|. \end{aligned} \quad (23)$$

Notably, the series of  $pp$  ladder diagrams is a divergent asymptotic series with zero radius of convergence [25, 39, 40]. The physical context of this so-called “renormalon divergence” is the Cooper pairing phenomenon [39]. Mathematically, the divergence is due to the singularities of  $\mathcal{J}_n^R(P, k)$  at the boundaries of the hole-line integrals (i.e., the Lebesgue dominated convergence theorem is not satisfied).<sup>2</sup>

### D. Multi-fermion scattering and logarithms

While the two-body scattering diagrams involve only UV power divergences [see Sec. II B], multi-fermion scattering involves also logarithmic divergences  $\sim \ln(\Lambda/Q)$ , where  $Q$  is an invariant kinematical variable. For scattering diagrams,  $Q$  is an external momentum, and in MBPT at zero temperature  $Q$  is the Fermi momentum  $k_F$ . That is, logarithmic UV divergences appear with a ratio of scales, which implies that their coefficients must be regulator independent (in contrast to the coefficients of UV power divergences), see also Ref. [11]. Renormalization removes the dependence on the UV cutoff  $\Lambda$  such that the logarithms become  $\ln(\Lambda_0/Q)$ , where  $\Lambda_0$  is an arbitrary auxiliary scale [see Sec. IV for details]. The dependence on  $\Lambda_0$  is canceled by the “running” with  $\Lambda_0$  of the many-body coupling  $g_j$  associated with the respective counterterm. Note that this cancellation requires that the involved terms are kept together, i.e., independent partial resummations are inhibited by the requirement of  $\Lambda_0$  independence.

For  $g > 2$ , the first logarithms in perturbative  $N$ -body scattering (for  $N \geq 3$ ) appear from the  $C_0$  interaction at order  $3N - 5$ , i.e., at fourth order in the three-body sector. (The first momentum-dependent logarithmic divergence appears at order  $3N - 3$  and is renormalized by  $D_2$ , etc., conforming to the perturbative EFT power counting.) The fourth-order three-body scattering diagrams with logarithmic divergences,  $\Gamma_1$  and  $\Gamma_2$ , are shown in Fig. 2; the associated many-body diagrams are listed in Fig. 3. They are renormalized by the contributions from

the leading three-body contact interaction with coupling  $D_0$  (corresponding to the last diagram in Fig. 2). This requires that the cutoff dependence of the  $D_0$  coupling is then given by

$$D_0(\Lambda) = D_0(\Lambda_0) + \eta M^3 C_0^4 \ln(\Lambda/\Lambda_0). \quad (24)$$

The regulator-independent coefficient  $\eta$  is obtained from the evaluation of the diagrams  $\Gamma_1$  and  $\Gamma_2$  (plus the bubble-counterterm diagram  $\Gamma_2^{\text{ct}}$ ) of Fig. 2, or equivalently, from the evaluation of the corresponding many-body diagrams; see Sec. IV for details. The dependence of the first term  $D_0(\Lambda_0)$  is such that  $D_0(\Lambda)$  is independent of the auxiliary scale  $\Lambda_0$ . The value of  $D_0(\Lambda_0)$  has to be fixed (for a given choice of  $\Lambda_0$ ) by matching to few- or many-body data.

For  $g = 2$ , all logarithmic divergences from  $S$ -wave interactions cancel, as required by the Pauli principle (the leading three-body contact interactions are Pauli blocked for  $g = 2$ ). That is, for  $g = 2$  the  $S$ -wave part of the MBPT series is completely determined by two-body scattering (i.e., by the ERE). For  $P$ -wave interactions or  $S$ -wave interactions in  $g > 2$  systems on the other hand, an increasing number of  $N$ -body couplings is needed for perturbative renormalization beyond the two-body sector.

Finally, we note that the contact interactions between fermions can be rewritten such that they involve the propagation of (so-called) dimer fields, and carrying out the partial diagrammatic resummations that renormalize the dimer propagator makes the  $C_0$  part of the perturbation series for three-body scattering UV finite also for  $g > 2$  [43]. Nevertheless, to achieve cutoff independence of the integral equation that corresponds to resumming the remaining diagrams requires to include the leading three-body coupling  $D_0$  (but no higher-order three-body interactions) [43, 44]. (Perturbatively expanding the nonperturbative three-body scattering amplitude then allows one to determine the perturbative  $D_0$  from nonperturbative three-body data [45].) Beyond the two-body sector, the relation of the nonperturbative renormalization of the  $C_0$  interaction (with a single three-body coupling  $D_0$ ) to the perturbative case, which requires in addition to  $C_0$  and  $D_0$  also many-body contact interactions at higher orders, is thus nontrivial, and a general understanding of this issue is still missing [46].

### E. Resummations for large scattering length

If there is a two-body bound-state at threshold the  $S$ -wave scattering length  $a_s$  is unnaturally large, and in this case the perturbative EFT expansion is of limited use. In the two-body sector, this case can be straightforwardly dealt with by resumming the  $C_0$  contributions and adding  $C_2, \dots$  perturbatively, which leads to [29, 38]

$$T^{(s)}(k) = \frac{1}{\frac{1}{a_s} + ik} + \frac{r_s k^2}{\left(\frac{1}{a_s} + ik\right)^2} + \dots \quad (25)$$

<sup>2</sup> Note that (in contrast to, e.g., relativistic  $\phi^4$  theory [41]) the renormalon divergence occurs for both the renormalized and the regularized perturbation series. The MBPT series has still zero radius convergence if the ladders are resummed [39, 42]; the large-order behavior is however (expected to be) dominated by renormalons [39].

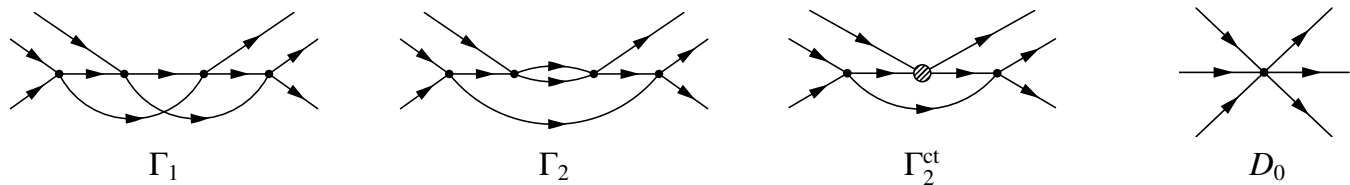


Figure 2. The first three-body scattering diagrams with logarithmic divergences  $\Gamma_1$  and  $\Gamma_2$ . Also shown is the counterterm diagram  $\Gamma_2^{\text{ct}}$  for the  $pp$  bubble of  $\Gamma_2$  (the counterterm is depicted as a shaded blob). The fourth diagram is the leading three-body contact contribution in three-fermion scattering, which includes the counterterm for the logarithmic UV divergences of  $\Gamma_1$  and  $\Gamma_2$ . Closing the external lines one obtains from  $\Gamma_1$  and  $\Gamma_2$  the MBPT diagrams with logarithmic divergences II5, II6, IIA1, and III1 shown in Fig. 3 below. See Sec. IV for details on the evaluation of these diagrams.

Such a simple analytic resummation of the  $C_0$  contributions is however not possible for the much more complicated MBPT series. A notable benchmark for nonperturbative many-body treatments of the  $C_0$  term is given by the  $a_s \rightarrow \infty$  limit, corresponding to the unitary Fermi gas. From dimensional analysis it follows that the ground-state energy density of the unitary Fermi gas of spin one-half fermions is given by  $E(k_F) = \xi E_0(k_F)$ , where  $E_0(k_F) = k_F^5 / (10\pi^2 M)$  is the noninteracting ground-state energy density and  $\xi$  is the Bertsch parameter. From experiments with ultracold atoms [2], the value  $\xi \approx 0.376(4)$  has been inferred.

The most straightforward nonperturbative many-body approximation consists of resumming a subclass of MBPT diagrams. The analytic resummation of the particle-particle ( $pp$ ) ladders gives  $\xi_{pp} \approx 0.237$  [33, 47], and resumming also hole-hole ( $hh$ ) and mixed  $pp$ - $hh$  ladders gives  $\xi_{\text{ladders}} \approx 0.5076$  [47].<sup>3</sup> In addition, a value for  $\xi_\epsilon \approx 0.475$  was deduced in Ref. [49] by expanding in terms of  $\epsilon = 4 - d$ , where  $d$  is the number of space dimensions, and subsequently interpolating between the  $\epsilon = 2$  and  $\epsilon = 0$  results for  $E(k_F)$ . Even more close comes the value  $\xi_{\text{LW}} \approx 0.36$  obtained from a self-consistent Luttinger-Ward type approach with resummed ladders [50] (see also Ref. [51]). (See also Ref. [42] for finite-temperature calculations based on Borel-resummed diagrammatic Monte Carlo calculations.) The most accurate value has been obtained from QMC computations,  $\xi_{\text{QMC}} = 0.372(5)$  [7].

Predictions for  $\xi$  may also be obtained by applying resummation methods such as Padé approximants to the  $a_s$  part of the Fermi-momentum expansion [52, 53]. We will present results from this approach in Sec. VI B.

### III. FOURTH-ORDER TERM FOR SPIN ONE-HALF FERMIONS

We now start with the discussion of the perturbative EFT expansion for dilute many-fermion systems at fourth order. Logarithms and many-body interactions

arise only for spin multiplicities  $g > 2$ , the intricacies of this case are postponed until Sec. IV. Here, we discuss the spin one-half case,  $g = 2$ , but we leave the notation general such that the results not affected by logarithmic terms can be carried over to  $g > 2$ . There are two different types of contributions at fourth order: (i) the second-order MBPT diagram with one  $C_0$  and one  $C_2$  vertex, and (ii) fourth-order MBPT diagrams with four  $C_0$  vertices (for  $g > 2$  there is also the first-order diagram with the  $D_0$  vertex). In each case, (in cutoff regularization) one has also two-body counterterm contributions from lower-order MBPT diagrams.

For the calculation of the contribution (i), see Refs. [28, 54]. The calculation of the contribution (ii) is much more involved. Among the possible MBPT diagrams with four  $C_0$  vertices, only those without single-vertex loops have to be considered at zero temperature. This is because all diagrams with single-vertex loops are removed by first-order mean-field (i.e., Hartree-Fock) insertions [55], and for a momentum-independent interaction, first-order mean-field renormalization at zero temperature has no effect for a uniform system. Therefore, as can easily be verified explicitly, these diagrams cancel each other at each order. The 39 remaining fourth-order many-body diagrams can be divided into four topological species:

- I(1-6): ladder diagrams,
- IA(1-3): ring diagrams,
- II(1-12), IIA(1-6): other two-particle irreducible diagrams,
- III(1-12): two-particle reducible diagrams,

where we have labeled diagrams according to groups that are closed under permutations of the vertices: I(1-6), IA(1-3), II(1-12), IIA(1-6), III(1-12). Diagrams III(3,6,11,12) are anomalous and thus give no contribution in zero-temperature MBPT [55, 56]. The 33 remaining diagrams are shown in Fig. 3.

Diagrams I1, I6, and IA1 are the fourth-order versions of the third-order  $pp$ ,  $hh$ , and  $ph$  diagrams; see, e.g., Ref. [57]. Diagrams I(2-5) are mixed  $pp$ - $hh$  ladder diagrams. The diagrams in the pairs I(3,4), III(7,8) and III(9,10) can be combined to get simplified energy denominators; I(2,5), II(1,2), II(3,4), II(7,8), II(11,12) and

<sup>3</sup> The resummation of particle-hole ladders (“ring diagrams”) becomes relevant for large values of  $g$ , in particular regarding the expansion about the large- $g$  limit [48].



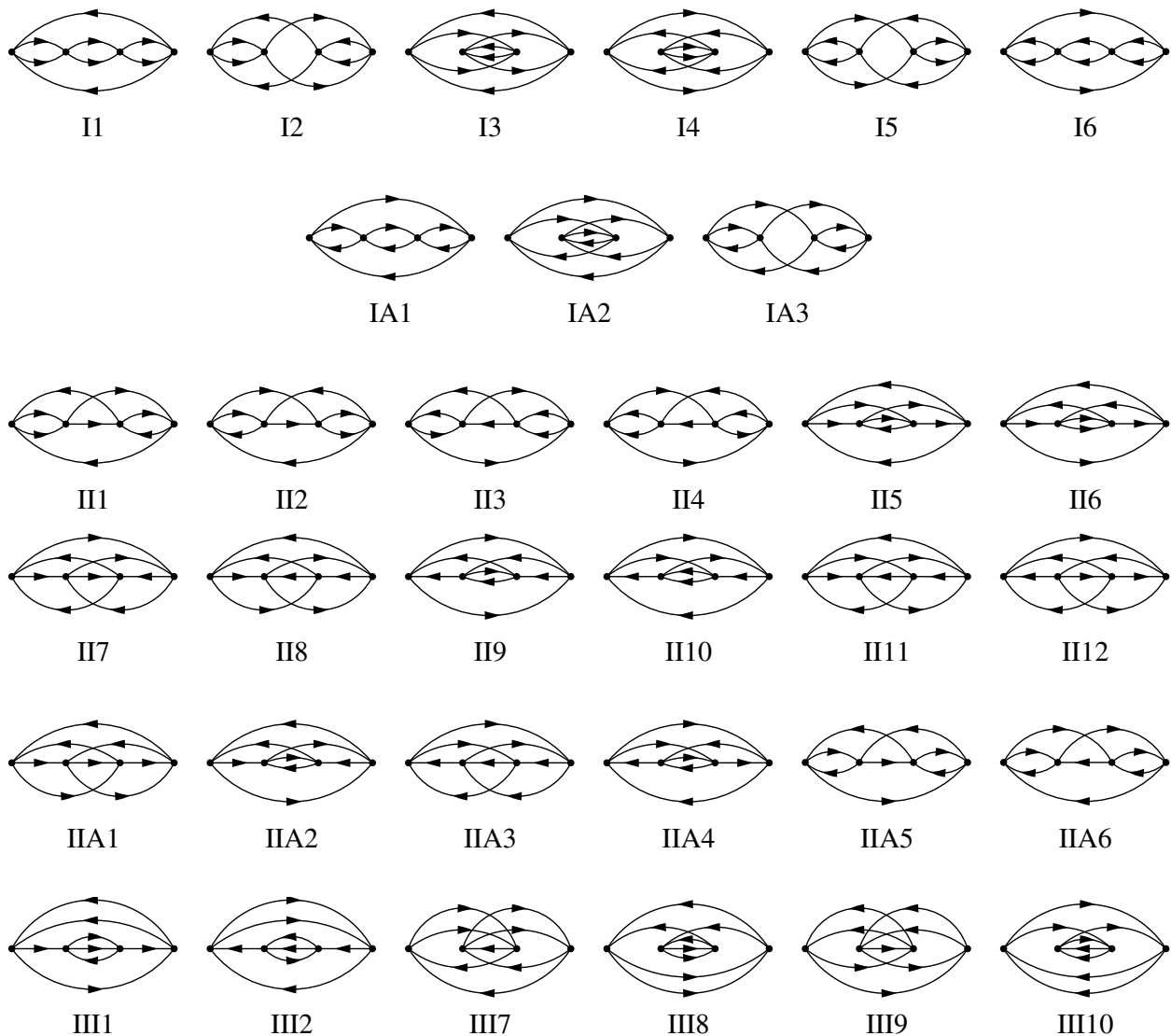


Figure 3. The 33 fourth-order Hugenholtz diagrams I(1-6), IA(1-3), II(1-12), IIA(1-6), and III(1,2,7-10). Diagrams II5 and IIA1 (corresponding to  $\Gamma_1$ ) as well as II6 and III1 (corresponding to  $\Gamma_2$ ) have logarithmic UV divergences.

IIA(2,4) give identical results for a spin-independent potential; and for a momentum-independent potential the contribution from I(3+4) is half of that from I(2+5).

The ladder diagrams I(1-6) are most conveniently computed by expanding the semianalytic formula for the ladder resummation derived by Kaiser [47]. The expressions obtained in this way can be derived from the usual many-body expressions by introducing relative momentum coordinates and applying various partial-fraction decompositions as well as the Poincaré-Bertrand transformation formula [58]. For the numerical evaluation of the IA diagrams, it is more convenient to use single-particle momenta instead of relative momenta, because then the phase space is less complicated. The II, IIA and III diagrams without divergences can be evaluated in the same way as the IA diagrams. The following diagrams involve divergences:

- I(1,2,4,5), II(1,2,6), III(1,8): UV power divergences,
- II(5,6), IIA1, III1: logarithmic UV divergences,
- III(1,2,8,10): energy-denominator divergences.

The UV power divergences, corresponding to  $pp$  bubbles, are renormalized in terms of (low-order) diagrams with two-body counterterm vertices. For  $g = 2$ , the logarithmic UV divergences cancel in the sums II5+IIA1 and II6+III1. Finally, the energy-denominator divergences correspond to higher-order poles at the integration boundary; they cancel in the sums III(1+8) and III(2+10).

The counterterms for power divergences can be implemented by performing subtractions in the bubble parts of the integrands. For example, using a sharp cutoff,

$f(p/\Lambda) = \theta(\Lambda - p)$ , and scaling all momenta by a factor  $k_F$ , the regularized expression for  $\text{II}(1+2)$  is given by

$$E_{4,\text{II}(1+2)}(\Lambda) = -\zeta(g-3) \sum_{\mathbf{i},\mathbf{j},\mathbf{k}} \theta_{\mathbf{cd}} \theta_{\mathbf{kc}} \theta_{\mathbf{je}} \theta_{\mathbf{de}} \frac{n_{ijk} \bar{n}_{cde}}{\mathcal{D}_{cd,ij} \mathcal{D}_{de,ik}} \\ \times \sum_{\mathbf{a}} \theta_{\mathbf{ab}} \frac{\bar{n}_{ab}}{\mathcal{D}_{ab,ij}} \Big|_{\substack{\mathbf{b}=\mathbf{i}+\mathbf{j}-\mathbf{a} \\ \mathbf{c}=\mathbf{i}+\mathbf{j}-\mathbf{d} \\ \mathbf{e}=\mathbf{i}+\mathbf{k}-\mathbf{d}}} \quad (26)$$

Here,  $\sum_{\mathbf{i}} \equiv \int d^3i/(2\pi)^3$ , the distribution functions are  $n_{ij\dots} \equiv n_i n_j \dots$  and  $\bar{n}_{ab\dots} \equiv \bar{n}_a \bar{n}_b \dots$ , with  $n_i \equiv \theta(1-i)$  and  $\bar{n}_a \equiv \theta(a-1)$ , and the energy denominators are given by  $\mathcal{D}_{ab,ij} \equiv (a^2 + b^2 - i^2 - j^2)/(2M)$ . Moreover,  $\zeta = k_F^9 g(g-1) C_0^4$ , and  $\theta_{\mathbf{ab}} \equiv \theta(\Lambda/k_F - |\mathbf{a} - \mathbf{b}|/2)$ . The dependence of a given MBPT diagram on  $g$  is obtained by inserting a factor  $\delta_{\sigma_1, \sigma'_1} \delta_{\sigma_2, \sigma'_2} - \delta_{\sigma_1, \sigma'_2} \delta_{\sigma_2, \sigma'_1}$  for each vertex and summing over the spins  $\sigma_1^{(i)}$ ,  $\sigma_2^{(i)}$  of the in- and outgoing lines. (For  $P$ -wave interactions the factor is  $\delta_{\sigma_1, \sigma'_1} \delta_{\sigma_2, \sigma'_2} + \delta_{\sigma_1, \sigma'_2} \delta_{\sigma_2, \sigma'_1}$ .) For details on the diagrammatic rules, see, e.g., Ref. [11, 59]. The renormalized expression is given by<sup>4</sup>

$$E_{4,\text{II}(1+2)}^{\text{R}} = -\zeta(g-3) \sum_{\mathbf{i},\mathbf{j},\mathbf{k}} \frac{n_{ijk} \bar{n}_{cde}}{\mathcal{D}_{cd,ij} \mathcal{D}_{de,ik}} \\ \times \left[ \frac{\bar{n}_{ab}}{\mathcal{D}_{ab,ij}} - \frac{1}{\mathcal{D}_{aa,00}} \right] \Big|_{\substack{\mathbf{c}=\mathbf{i}+\mathbf{j}-\mathbf{d} \\ \mathbf{e}=\mathbf{i}+\mathbf{k}-\mathbf{d} \\ \mathbf{b}=\mathbf{i}+\mathbf{j}-\mathbf{a}}} \quad (27)$$

where the part  $\sim 1/\mathcal{D}_{aa,00}$  corresponds to the counterterm contribution. This expression can be further simplified such that only one unbounded integral appears, i.e., using

$$\sum_{\mathbf{a}} \left[ \frac{\bar{n}_{ab}}{\mathcal{D}_{ab,ij}} - \frac{1}{\mathcal{D}_{aa,00}} \right] = - \sum_{\mathbf{a}} \frac{n_a + n_b - n_{ab}}{\mathcal{D}_{ab,ij}} \quad (28)$$

we find

$$E_{4,\text{II}(1+2)}^{\text{R}} = 2\zeta(g-3) \sum_{\mathbf{i},\mathbf{j},\mathbf{k},\mathbf{a}} \frac{n_{ijka} \bar{n}_{cde}}{\mathcal{D}_{cd,ij} \mathcal{D}_{de,ik} \mathcal{D}_{ab,ij}} \frac{\mathcal{P}}{\mathcal{D}_{ab,ij}} \Big|_{\substack{\mathbf{c}=\mathbf{i}+\mathbf{j}-\mathbf{d} \\ \mathbf{e}=\mathbf{i}+\mathbf{k}-\mathbf{d} \\ \mathbf{b}=\mathbf{i}+\mathbf{j}-\mathbf{a}}} \quad (29)$$

where  $\mathcal{P}$  denote the Cauchy principal value. The direct application of Eq. (28) is prohibited for  $\text{II6}$  and  $\text{III1}$ , because in that case the pertinent energy denominators involve additional particle momenta. The regularized expression for  $\text{II6}$  is given by

$$E_{4,\text{II6}}(\Lambda) = -\zeta(g-3) \sum_{\mathbf{i},\mathbf{j},\mathbf{k}} \theta_{\mathbf{ab}} \theta_{\mathbf{ka}} \theta_{\mathbf{cd}} \theta_{\mathbf{je}} \theta_{\mathbf{be}} \\ \times \frac{n_{ijk} \bar{n}_{abcde}}{\mathcal{D}_{ab,ij} \mathcal{D}_{be,ik} \mathcal{D}_{bcd,ijk}} \Big|_{\substack{\mathbf{b}=\mathbf{i}+\mathbf{j}-\mathbf{a} \\ \mathbf{d}=\mathbf{k}+\mathbf{a}-\mathbf{c} \\ \mathbf{e}=\mathbf{k}+\mathbf{a}-\mathbf{j}}} \quad (30)$$

Substituting  $\mathbf{K} = (\mathbf{i} + \mathbf{j})/2$ ,  $\mathbf{p} = (\mathbf{i} - \mathbf{j})/2$ ,  $\mathbf{z} = \mathbf{k}$ ,  $\mathbf{A} = (\mathbf{a} - \mathbf{b})/2$ , and  $\mathbf{Y} = (\mathbf{c} - \mathbf{d})/2$ , and omitting redundant regulator functions, we have

$$E_{4,\text{II6}}(\Lambda) = -8M^3 \zeta(g-3) \sum_{\substack{\mathbf{K},\mathbf{p},\mathbf{z} \\ \mathbf{A},\mathbf{Y}}} n_{ijk} \bar{n}_{abcde} \theta_{\mathbf{A}} \theta_{\mathbf{Y}} \frac{1}{A^2 - p^2} \\ \times \frac{1}{(\mathbf{A} + \mathbf{p}) \cdot (\mathbf{A} - \mathbf{K} + \mathbf{z})} \frac{1}{Y^2 + \mathcal{R}}, \quad (31)$$

where  $\mathcal{R} = (3\mathbf{A} + \mathbf{K} - \mathbf{z}) \cdot (\mathbf{A} - \mathbf{K} + \mathbf{z})/4 - p^2$ . The UV power subdivergence can now be separated via

$$\frac{1}{Y^2 - p^2 + \mathcal{R}} = \underbrace{\frac{1}{Y^2}}_{\sim E_{4,\text{II6}(i)}} - \underbrace{\frac{\mathcal{R}}{(Y^2 + \mathcal{R})Y^2}}_{\sim E_{4,\text{II6}(ii)}} \quad (32)$$

For the UV power divergence of  $\text{II6}(i)$ , the counterterm can be implemented analogous to Eq. (28). The second part  $\text{II6}(ii)$  is only logarithmically UV divergent. For  $g=2$ , the logarithmic divergence is canceled if we add the  $\text{III1}$  term, which requires (due to the energy-denominator divergence) to add also  $\text{III}(7+8)$ . The regularized expression for  $\text{III}(1+7+8)$  is given by

$$E_{4,\text{III}(1+7+8)}(\Lambda) = -\zeta(g-1) \sum_{\mathbf{i},\mathbf{j},\mathbf{k}} \theta_{\mathbf{ab}} \theta_{\mathbf{ab}} \frac{n_{ijk} \bar{n}_{abc}}{\mathcal{D}_{ab,ij}^2} \\ \times \left( \theta_{\mathbf{ka}} \theta_{\mathbf{cd}} \frac{\bar{n}_d}{\mathcal{D}_{bcd,ijk}} - \theta_{\mathbf{cd}'} \frac{\bar{n}_{d'}}{\mathcal{D}_{cd',ik}} \right) \Big|_{\substack{\mathbf{b}=\mathbf{i}+\mathbf{j}-\mathbf{a} \\ \mathbf{d}=\mathbf{k}+\mathbf{a}-\mathbf{c} \\ \mathbf{d}'=\mathbf{i}+\mathbf{k}-\mathbf{c}}} \quad (33)$$

The energy-denominator divergence corresponds to  $\mathcal{D}_{ab,ij} = 0$ , and in that case the two terms in the large parentheses cancel each other. For  $\text{III}(1+8)$  also the linear UV divergences are removed.<sup>5</sup> For  $g=2$ , the contribution from the sum  $\text{II6}(ii)+\text{III}(1+7+8)$  is then given by

$$E_{4,\text{II6}(ii)+\text{III}(1+7+8)}^{\text{R}} \Big|_{g=2} = -8M^3 \zeta \sum_{\substack{\mathbf{K},\mathbf{p},\mathbf{z} \\ \mathbf{A},\mathbf{Y}}} \frac{n_{ijk} \bar{n}_{abc}}{A^2 - p^2} \times \mathcal{G}, \quad (34)$$

with

$$\mathcal{G} = \frac{1}{(\mathbf{A} + \mathbf{p}) \cdot (\mathbf{A} - \mathbf{K} + \mathbf{z})} \frac{\mathcal{R}}{(Y^2 + \mathcal{R})Y^2} \\ + \frac{1}{A^2 - p^2} \left[ \frac{1}{Y^2 + \mathcal{R}} - \frac{1}{Y^2 + \mathcal{R}'} \right], \quad (35)$$

<sup>4</sup> Throughout the paper, we label the cutoff-independent renormalized expressions corresponding to UV divergent diagrams with a subscript ‘‘R’’.

<sup>5</sup> The counterterms for the power divergences of  $\text{III1}$  and  $\text{III8}$  would come from diagrams with single-vertex loops.

where  $\mathcal{R}' = -(\mathbf{K} + \mathbf{p} - \mathbf{Z})^2/4$ . Finally, the regularized expressions for II5 and IIA1 are given by

$$E_{4,\text{II5}}(\Lambda) = -\zeta(g-3) \sum_{\substack{i,j,k \\ a,c}} \theta_{ab} \theta_{kb} \theta_{cd} \theta_{ad} \theta_{ke} \theta_{ce} \\ \times \frac{n_{ijk} \bar{n}_{abcde}}{\mathcal{D}_{ab,ij} \mathcal{D}_{ce,ij} \mathcal{D}_{acd,ijk}} \Big|_{\substack{b=i+j-a \\ d=i+j+k-a-c \\ e=i+j-c}}, \quad (36)$$

$$E_{4,\text{IIA1}}(\Lambda) = -\zeta(3g-5) \sum_{\substack{i,j,k \\ a,c}} \theta_{ab} \theta_{kb} \theta_{cd} \theta_{ad} \theta_{je} \theta_{ce} \\ \times \frac{n_{ijk} \bar{n}_{abcde}}{\mathcal{D}_{ab,ij} \mathcal{D}_{ce,ik} \mathcal{D}_{acd,ijk}} \Big|_{\substack{b=i+j-a \\ d=i+j+k-a-c \\ e=i+k-c}}. \quad (37)$$

For  $g = 2$ , the sum of these contribution is UV finite, and is given by

$$E_{4,\text{II5+IIA1}}^{\text{R}}|_{g=2} = \zeta \sum_{\substack{i,j,k \\ a,c}} \frac{n_{ijk} \bar{n}_{abcd}}{\mathcal{D}_{ab,ij} \mathcal{D}_{acd,ijk}} \Big|_{\substack{b=i+j-a \\ d=i+j+k-a-c}} \\ \times \left( \frac{\bar{n}_e}{\mathcal{D}_{ce,ij}} \Big|_{e=i+j-c} - \frac{\bar{n}_{e'}}{\mathcal{D}_{ce',ik}} \Big|_{e'=i+k-c} \right). \quad (38)$$

The contributions from II5+IIA1 as well as II6(ii)+II(1+7+8) can of course also be evaluated by subtracting the individual logarithmic divergences, i.e., by adding the respective (counterterm) parts of  $D_0(\Lambda)$  (only the sum of these parts vanishes for  $g = 2$ ), see Sec. IV. We have however found that evaluating the sums II5+IIA1 and II6(ii)+II(1+7+8) provides better numerical precision (see Table I).

#### IV. FOURTH-ORDER TERM FOR HIGHER SPINS

For  $g > 2$ , the logarithmic divergences of II6, IIA1, II5 and III(1+7+8) are canceled by the contribution from the first-order MBPT diagram with  $D_0$  vertex. In cutoff regularization, this cancellation is tantamount to

$$\Lambda \frac{\partial}{\partial \Lambda} D_0(\Lambda) = \eta M^3 C_0^4, \quad (39)$$

where the coefficient  $\eta$  is determined by the logarithmic UV divergence. This can be integrated as

$$D_0(\Lambda) = D_0(\Lambda_0) + \eta M^3 C_0^4 \ln(\Lambda/\Lambda_0), \quad (40)$$

where  $\Lambda_0$  is an arbitrary auxiliary scale, and  $D_0(\Lambda)$  is independent of  $\Lambda_0$ , as evident from the running with  $\Lambda_0$  according to Eq. (39) of the integration constant  $D_0(\Lambda_0)$ :  $D_0(\Lambda'_0) = D_0(\Lambda_0) + \eta M^3 C_0^4 \ln(\Lambda'_0/\Lambda_0)$ . The value of  $D_0(\Lambda_0)$  has to be fixed (for a given choice of  $\Lambda_0$ ) by matching to few- or many-body data (see, e.g., Ref. [45]).

For further details we refer to the general discussion of logarithmic divergences in EFT provided in Sec. IID.

Below, we first show how the fourth-order term for  $g > 2$  is calculated in cutoff regularization, and then discuss the calculation in dimensional regularization (DR). The pendant of Eq. (39) in DR is given by Eq. (85) below.

#### A. Cutoff regularization

The coefficient  $\eta = \eta_1 + \eta_2$  is determined by the logarithmic divergence of II6+IIA1+II5+III(1+7+8), or equivalently, by the logarithmic divergence of the three-body scattering diagrams  $\Gamma_1$  and  $\Gamma_2$  (see Fig. 2). Using a sharp cutoff,  $f(p/\Lambda) = \theta(\Lambda - p)$ , the regularized expression for diagram  $\Gamma_1$  is given by

$$\Gamma_1(\Lambda) = -\frac{3^3 2^4}{3!} C_0^4 \mathcal{J}_1(\Lambda), \quad (41)$$

with

$$\mathcal{J}_1(\Lambda) = \sum_{\mathbf{x}_1, \mathbf{x}_2, \mathbf{x}_3, l_1, l_2} \theta_{\mathbf{x}_1 l_1} \theta_{\mathbf{x}_1 k_1} \theta_{\mathbf{x}_2 l_1} \theta_{\mathbf{x}_2 l_2} \theta_{\mathbf{x}_3 l_2} \theta_{\mathbf{x}_3 k'_3} \\ \times \frac{1}{\mathcal{D}_{x_1 l_1, k_2 k_3}^* \mathcal{D}_{x_2 l_1 l_2, k_1 k_2 k_3}^* \mathcal{D}_{x_3 l_2, k'_1 k'_2}^*} \\ \times \delta_{\mathbf{x}_1 l_1, k_2 k_3} \delta_{\mathbf{x}_2 l_1 l_2, k_1 k_2 k_3} \delta_{\mathbf{x}_3 l_2, k'_1 k'_2}, \quad (42)$$

where  $\mathbf{k}_{1,2,3}$  and  $\mathbf{k}'_{1,2,3}$  are the three-momenta of the in- and outgoing particles, respectively, with  $\mathbf{k}_1 + \mathbf{k}_2 + \mathbf{k}_3 = \mathbf{k}'_1 + \mathbf{k}'_2 + \mathbf{k}'_3$ , and  $\mathbf{x}_{1,2,3}$  and  $l_{1,2}$  are the loop momenta, and  $\mathcal{D}^* = \mathcal{D} - i\epsilon$ . The factor  $3^3$  comes from cyclic permutations of the initial and final lines, the factor  $2^4$  is due to the number of equivalent contractions for a given choice of final and initial lines, and the factor  $1/3!$  is due to final-state antisymmetrization. Similarly, the regularized expression for the sum of diagrams  $\Gamma_2$  and  $\Gamma_2^{\text{ct}}$  of Fig. 2 is given by

$$[\Gamma_2 + \Gamma_2^{\text{ct}}](\Lambda) = -\frac{3^2 2^3}{3!} C_0^4 \mathcal{J}_2(\Lambda), \quad (43)$$

with

$$\mathcal{J}_2(\Lambda) = \sum_{\mathbf{x}_1, \mathbf{x}_2, \mathbf{x}_3, l_1, l_2} \theta_{\mathbf{x}_1 l_1} \theta_{\mathbf{x}_1 k_1} \theta_{\mathbf{x}_2 l_2} \theta_{\mathbf{x}_3 l_2} \theta_{\mathbf{x}_3 k'_1} \\ \times \frac{1}{\mathcal{D}_{x_1 l_1, k_1 k_2}^* \mathcal{D}_{x_3 l_1, k'_1 k'_2}^*} \left[ \frac{1}{\mathcal{D}_{x_2 l_1 l_2, k_1 k_2 k_3}^*} - \frac{1}{\mathcal{D}_{l_2 l_2}^*} \right] \\ \times \delta_{\mathbf{x}_1 l_1, k_2 k_3} \delta_{\mathbf{x}_2 l_1 l_2, k_1 k_2 k_3} \delta_{\mathbf{x}_3 l_1, k'_1 k'_2}, \quad (44)$$

where the term in squared brackets involves the counterterm for the two-particle bubble. Overall, the logarithmic divergence is given by

$$\Gamma_1(\Lambda) \xrightarrow{\Lambda \rightarrow \infty} -\eta_1 M^3 C_0^4 \ln(\Lambda), \quad (45)$$

$$[\Gamma_2 + \Gamma_2^{\text{ct}}](\Lambda) \xrightarrow{\Lambda \rightarrow \infty} -\eta_2 M^3 C_0^4 \ln(\Lambda). \quad (46)$$



To determine  $\eta_{1,2}$  we can set all external momenta to zero, i.e.,

$$\mathcal{J}_{1,2}(\Lambda) \xrightarrow{\mathbf{k}_{1,2,3} \rightarrow 0} M^3 \mathcal{I}_{1,2}(\Lambda). \quad (47)$$

Introducing relative momenta  $\mathbf{q}_1$  and  $\mathbf{q}_2$  such that  $\{\mathbf{1}_{1,2}, \mathbf{x}_{1,2,3}\} = \{\mathbf{q}_1, (\mathbf{q}_1 + 2\mathbf{q}_2)/2, \mathbf{q}_1, (\mathbf{q}_1 - 2\mathbf{q}_2)/2, -\mathbf{q}_1\}$ , the integral  $\mathcal{I}_2(\Lambda)$  is given by

$$\mathcal{I}_2(\Lambda) = \int_{\aleph}^{\Lambda} \frac{d^3 q_1}{(2\pi)^3} \int_{\aleph}^{\Lambda} \frac{d^3 q_2}{(2\pi)^3} \frac{1}{q_1^4} \left[ \frac{1}{3q_1^2/4 + q_2^2} - \frac{1}{q_2^2} \right], \quad (48)$$

where the integral boundaries are with respect to the radial coordinates. To have an infrared finite expression we have, as a formal intermediate step, introduced an arbitrary infrared cutoff  $\aleph$ . This integral can be expressed in terms of the inverse tangent integral  $\text{Ti}_2(x) = [\text{Li}_2(ix) - \text{Li}_2(ix)]/(2i)$ , with  $\text{Li}_2(z)$  the complex dilogarithm, i.e.,

$$-\frac{3^3 2^4}{3!} \mathcal{I}_2(\Lambda) = -\frac{\sqrt{3}}{2^3 \pi^4} \text{Ti}_2 \left( \frac{2q_2}{\sqrt{3}q_1} \right) \Big|_{\aleph, \aleph}^{\Lambda, \Lambda}. \quad (49)$$

Using  $\text{Ti}_2(x) = \text{Ti}_2(1/x) + (\pi/2)\text{sgn}(x) \ln x$  as well as  $\text{Ti}_2(0) = 0$  we find (for  $\aleph \rightarrow 0$ )

$$\eta_2 = -\frac{3\sqrt{3}}{4\pi^3}. \quad (50)$$

For  $\Gamma_1$ , this method to extract logarithms is prohibited by the  $\theta_{\mathbf{x}_{312}}$  factor and a nontrivial angular integral. This problem can be avoided in DR where loop integrals remain invariant under translations of the integration variables. As shown in Sec. IV B, one obtains

$$\eta_1 = \frac{1}{\pi^2}. \quad (51)$$

From this, the renormalized fourth-order contribution to the ground-state energy is

$$E_4(k_F) = \chi [D_0(\Lambda_0) + \eta M^3 C_0^4 \ln(k_F/\Lambda_0)] + \sum_i E_{4,i}^R + \dots, \quad (52)$$

where  $i \in \{\text{II5}, \text{IIA1}, \text{II6}, \text{III}(1+7+8)\}$ , and the ellipses refer to contributions from other fourth-order diagrams. The factor  $\chi$  corresponding to the first-order three-body diagram is

$$\chi = \frac{g(g-1)(g-2)}{6} \sum_{ijk} n_{ijk} = \alpha(g-2) \frac{M}{108\pi^4 a_s^4}, \quad (53)$$

with  $\alpha = n\varepsilon_F(k_F a_s)^4(g-1)$ , where  $n = g k_F^3/(6\pi^2)$  is the fermion number density and  $\varepsilon_F = k_F^2/(2M)$  the noninteracting Fermi energy. Finally, the terms  $E_{4,i}^R$  are given

by<sup>6</sup>

$$E_{4,\text{II5}}^R = \lim_{\Lambda \rightarrow \infty} [E_{4,\text{II5}}(\Lambda) + (g-3)L_1(\Lambda)], \quad (54)$$

$$E_{4,\text{IIA1}}^R = \lim_{\Lambda \rightarrow \infty} [E_{4,\text{IIA1}}(\Lambda) + (3g-5)L_1(\Lambda)], \quad (55)$$

$$E_{4,\text{II6}}^R = \lim_{\Lambda \rightarrow \infty} \left[ E_{4,\text{II6(i)}}^R + E_{4,\text{II6(ii)}}^R(\Lambda) + (g-3)L_2(\Lambda) \right], \quad (56)$$

$$E_{4,\text{III}(1+7+8)}^R = \lim_{\Lambda \rightarrow \infty} [E_{4,\text{III}(1+7+8)}(\Lambda) + (g-1)L_2(\Lambda)]. \quad (57)$$

Here, the terms  $L_1(\Lambda)$  and  $L_2(\Lambda)$  cancel the logarithmic parts of the respective many-body diagrams,  $\sim \ln(\Lambda/k_F)$ , with  $4(g-2)L_1(\Lambda) + 2(g-2)L_2(\Lambda) = \chi \eta M^3 C_0^4 \ln(\Lambda/k_F)$  matching the form of the logarithm in Eq. (52). They are given by

$$L_1(\Lambda) = \alpha \frac{16}{27\pi^2} \ln(\Lambda/k_F), \quad (58)$$

$$L_2(\Lambda) = -\alpha \frac{8\sqrt{3}}{9\pi^3} \ln(\Lambda/k_F), \quad (59)$$

which matches (with different phase-space prefactors) the logarithmic parts of the three-body scattering integrals  $\mathcal{J}_1(\Lambda)$  and  $\mathcal{J}_2(\Lambda)$ , respectively. One finds that

$$E_{4,\text{II5}}^R = \alpha(g-3) \times 0.0645(1), \quad (60)$$

$$E_{4,\text{IIA1}}^R = \alpha(3g-5) \times 0.0647(1), \quad (61)$$

$$E_{4,\text{II6}}^R = -\alpha(g-3) \times 0.0265(2), \quad (62)$$

$$E_{4,\text{III}(1+7+8)}^R = -\alpha(g-1) \times 0.0513(2). \quad (63)$$

The sum of the first and second two contributions is given by

$$E_{4,\text{II5+IIA1}}^R = \alpha [0.00018(1) + (g-2) \times 0.2586(4)], \quad (64)$$

$$E_{4,\text{II6+III}(1+7+8)}^R = \alpha [-0.0248(1) - (g-2) \times 0.0778(3)], \quad (65)$$

where in each case the leading term corresponds to the result obtained in the  $g=2$  calculation of Sec. III.

## B. Dimensional regularization

The DR calculation of the logarithmic terms is similar to the calculation of the corresponding terms for bosonic systems carried out by Braaten and Nieto [60]. In DR,

<sup>6</sup> See Eq. (32) for the splitting of II6 into a power-divergent part II6(i) and a logarithmically divergent part II6(ii).

the coefficient of the logarithm arising from diagram  $\Gamma_1$  is determined by the integral

$$\mathcal{I}_1^D = \mu^{2(3-D)} \int \frac{d^D l_1}{(2\pi)^D} \int \frac{d^D l_2}{(2\pi)^D} \frac{1}{(l_1^2 + \aleph^2)} \times \frac{1}{(l_1^2 + l_2^2 + \mathbf{l}_1 \cdot \mathbf{l}_2 + \aleph^2)} \frac{1}{(l_2^2 + \aleph^2)}. \quad (66)$$

Here,  $\mu$  is a momentum scale introduced to maintain the correct mass dimension, and the scale  $\aleph$  serves to admit the use of Eq. (72) below. [Note that this is a different scale from the  $\aleph$  used in Sec. IV A within cutoff regularization.] Introducing Feynman parameters we obtain

$$\mathcal{I}_1^D = \mu^{2(3-D)} \int \frac{d^D l_1}{(2\pi)^D} \int \frac{d^D l_2}{(2\pi)^D} \int_0^1 dx \int_0^{1-x} dy \times \frac{2}{[l_1^2(x+y) + l_2^2(1-x) + \mathbf{l}_1 \cdot \mathbf{l}_2 y + \aleph^2]^3}. \quad (67)$$

Shifting  $\mathbf{l}_1 \rightarrow \mathbf{l}_1 - \mathbf{l}_2 y / (2x + 2y)$  and rescaling the integration variables leads to

$$\mathcal{I}_1^D = \mu^{2(3-D)} \mathcal{F}_1^D \int \frac{d^D l_1}{(2\pi)^D} \int \frac{d^D l_2}{(2\pi)^D} \frac{2}{(l_1^2 + l_2^2 + \aleph^2)^3}, \quad (68)$$

with

$$\mathcal{F}_1^D = \int_0^1 dx \int_0^{1-x} dy \left[ (x+y)(1-x) - \frac{y^2}{4} \right]^{-D/2}. \quad (69)$$

We can expand this in  $\epsilon = D - 3$ ,  $\mathcal{F}_1^{D=3+\epsilon} = \mathcal{F}_1 + \epsilon \mathcal{F}'_1 + \mathcal{O}(\epsilon^2)$ , with

$$\mathcal{F}_1 = \int_0^1 dx \int_0^{1-x} dy \left[ (x+y)(1-x) - \frac{y^2}{4} \right]^{-3/2} = \frac{4\pi}{3}, \quad (70)$$

$$\mathcal{F}'_1 = - \int_0^1 dx \int_0^{1-x} dy \frac{\ln \left( (x+y)((1-x) - \frac{y^2}{4}) \right)}{2 \left[ (x+y)(1-x) - \frac{y^2}{4} \right]^{3/2}} \approx 4.71849. \quad (71)$$

Applying the relation [36]

$$\int d^D q \frac{1}{(q^2 + \aleph^2)^n} = \pi^{D/2} \frac{1}{\aleph^{2n-D}} \frac{\Gamma(n-D/2)}{\Gamma(n)}, \quad (72)$$

and analytically continuing to  $D = 3 + \epsilon$ , we then find

$$\mathcal{I}_1^{D=3+\epsilon} = \frac{1}{48\pi^2} \left[ -\frac{1}{\epsilon} - 2 \ln(\aleph/\mu) + \zeta_1 + \mathcal{O}(\epsilon) \right], \quad (73)$$

where  $\zeta_1 = \ln(4\pi) - \gamma_E - 3\mathcal{F}'_1/(4\pi) \approx 0.827352$ , with  $\gamma_E \approx 0.577216$  the Euler-Mascheroni constant. This agrees with the corresponding result for bosonic systems

derived by Braaten and Nieto [60]. Note that for  $D = 3$  the left side of Eq. (72) is UV divergent for  $n \geq -3/2$ , but the right side is singular only for  $n = 3/2$ . This is the well-known feature that power divergences are automatically set to zero in DR.

Efimov [20] and Bishop [26] extracted the leading logarithms by introducing a cutoff  $\Lambda$  on one of the loop momenta  $\mathbf{l}_{1,2}$  only. DR makes it clear why this method gives the correct result: the analytic continuation  $D \rightarrow 3 + \epsilon$  can be performed for individual subintegrals individually. For diagrams with subdivergences this procedure would in fact be required to obtain finite results. This is the case for diagram  $\Gamma_2$ , where the divergent integral is

$$\mathcal{I}_{2,a}^D = \mu^{3-D} \int \frac{d^D l_1}{(2\pi)^D} \frac{1}{(l_1^2 + \aleph^2)} \frac{1}{(l_1^2 + \aleph^2)} \times \mu^{3-D} \int \frac{d^D l_2}{(2\pi)^D} \frac{1}{(l_1^2 + l_2^2 + \mathbf{l}_1 \cdot \mathbf{l}_2 + \aleph^2)}. \quad (74)$$

Shifting  $\mathbf{l}_2 \rightarrow \mathbf{l}_2 - \mathbf{l}_1/2$ , performing the  $\mathbf{l}_2$  integration, and analytic continuation to  $D = 3 + \epsilon$  leads to

$$\mathcal{I}_{2,a}^D = -\frac{\mu^{3-D}}{4\pi} \int \frac{d^D l_1}{(2\pi)^D} \frac{1}{(l_1^2 + \aleph^2)} \frac{1}{(l_1^2 + \aleph^2)} \sqrt{\frac{3}{4} l_1^2 + \aleph^2}, \quad (75)$$

which, for  $D = 3$ , indeed diverges only logarithmically in the UV.<sup>7</sup> Note that also the IR divergence (for  $\aleph = 0$ ,  $D = 3$ ) of the  $\mathbf{l}_2$  integrals has been eliminated. However, to get to a form where we can apply Eq. (72) we would proceed instead as

$$\mathcal{I}_{2,a}^D = \mu^{2(3-D)} \int \frac{d^D l_1}{(2\pi)^D} \int \frac{d^D l_2}{(2\pi)^D} \int_0^1 dx (1-x) \times \frac{2}{[l_1^2 + l_2^2 x + \mathbf{l}_1 \cdot \mathbf{l}_2 x + \aleph^2]^3}. \quad (76)$$

Shifting  $\mathbf{l}_1 \rightarrow \mathbf{l}_1 - \mathbf{l}_2 x/2$  and rescaling the integration variables leads to

$$\mathcal{I}_{2,a}^D = \mu^{2(3-D)} \mathcal{F}_{2,a}^D \int \frac{d^D l_1}{(2\pi)^D} \int \frac{d^D l_2}{(2\pi)^D} \frac{2}{(l_1^2 + l_2^2 + \aleph^2)^3}, \quad (77)$$

with

$$\mathcal{F}_{2,a}^D = \int_0^1 dx (1-x) \left[ x - \frac{x^2}{4} \right]^{-D/2}, \quad (78)$$

which is singular for  $D \geq 2$ , obviously a manifestation of the subdivergence. This singularity can be removed by

<sup>7</sup> In particular, setting  $D = 3$  and  $\aleph = 0$ , and introducing an UV cutoff on  $\mathbf{l}_1$  is equivalent to the calculations by Efimov [20] and Bishop [26].

adding the term

$$\mathcal{I}_{2,b}^D = -\mu^{2(3-D)} \int \frac{d^D l_1}{(2\pi)^D} \frac{1}{(l_1^2 + \aleph^2)} \frac{1}{(l_1^2 + \aleph^2)} \times \int \frac{d^D l_2}{(2\pi)^D} \frac{1}{(l_2^2 + \aleph^2)}, \quad (79)$$

i.e.,

$$\mathcal{I}_{2,b}^D = \mu^{2(3-D)} \mathcal{F}_{2,b}^D \int \frac{d^D l_1}{(2\pi)^D} \int \frac{d^D l_2}{(2\pi)^D} \frac{2}{(l_1^2 + l_2^2 + \aleph^2)^3}, \quad (80)$$

where

$$\mathcal{F}_{2,b}^D = - \int_0^1 dx (1-x) [x-x^2]^{-D/2} \quad (81)$$

is also singular for  $D \geq 2$ , but  $\mathcal{F}_2^D = \mathcal{F}_{2,a}^D + \mathcal{F}_{2,b}^D$  is finite. Expanding  $\mathcal{F}_2^{D=3+\epsilon} = \mathcal{F}_2 + \epsilon \mathcal{F}'_2 + \mathcal{O}(\epsilon)^2$ , where

$$\mathcal{F}_2 = -2\sqrt{3}, \quad (82)$$

$$\mathcal{F}'_2 = -\frac{8\pi}{3} - \sqrt{3}(\ln(4/3) - 2) \approx -5.41176, \quad (83)$$

we find for  $\mathcal{I}_2^D = \mathcal{I}_{2,a}^D + \mathcal{I}_{2,b}^D$ :

$$\mathcal{I}_2^D = -\frac{\sqrt{3}}{32\pi^3} \left[ -\frac{1}{\epsilon} - 2 \ln(\aleph/\mu) + \zeta_2 + \mathcal{O}(\epsilon) \right], \quad (84)$$

with  $\zeta_2 = \ln(4\pi) - \gamma_E + \mathcal{F}'_2/(2\sqrt{3}) \approx 0.39157$ . This again matches the corresponding result for bosons derived by Braaten and Nieto [60]. As required, the coefficient of  $\ln \mu$  matches the one of  $\ln \Lambda$  in the cutoff calculation, see Eq. (50).

Subtracting in Eqs. (73) and (84) only the divergent parts  $\sim 1/\epsilon$  corresponds to minimal subtraction (MS). The coupling  $D_0$  is then fixed as  $D_0 = D_0^*(\mu) + \eta M^3 C_0^4 / (2\epsilon)$ , where the scaling of  $D_0^*(\mu)$  with  $\mu$  is identical to the scaling of  $D_0(\Lambda_0)$  with  $\Lambda$ , i.e., instead of Eq. (39) we have

$$\mu \frac{\partial}{\partial \mu} D_0^*(\mu) = \eta M^3 C_0^4. \quad (85)$$

The couplings  $D_0^*(\mu)$  and  $D_0(\Lambda_0)$  are not identical for  $\mu = \Lambda_0$ , i.e., they differ in terms of a subtraction constant specific to the respective regularization and subtraction procedure. Instead of Eq. (52) we have

$$E_4(k_F) = \chi [D_0^*(\mu_0) + \eta M^3 C_0^4 \ln(k_F/\mu_0)] + \sum_i E_{4,i}^{\text{MS}} + \dots, \quad (86)$$

with<sup>8</sup>

$$E_{4,\text{II5}}^{\text{MS}} = E_{4,\text{II5}}(\aleph) + (g-3)L_1^*(\aleph), \quad (87)$$

$$E_{4,\text{IIA1}}^{\text{MS}} = E_{4,\text{IIA1}}(\aleph) + (3g-5)L_1^*(\aleph), \quad (88)$$

$$E_{4,\text{II6}}^{\text{MS}} = E_{4,\text{II6(i)}}^{\text{R}} + E_{4,\text{II6(ii)}}(\aleph) + (g-3)L_2^*(\aleph), \quad (89)$$

$$E_{4,\text{III}(1+7+8)}^{\text{MS}} = E_{4,\text{III}(1+7+8)}(\aleph) + (g-1)L_1^*(\aleph), \quad (90)$$

where  $4L_1^*(\aleph) + 2L_2^*(\aleph) = \chi \eta M^3 C_0^4 \ln(\aleph/k_F)$ , with

$$L_1^*(\aleph) = \alpha \frac{16}{27\pi^2} \left[ \frac{\zeta_1}{2} + \ln(\aleph/k_F) \right], \quad (91)$$

$$L_2^*(\aleph) = -\alpha \frac{8\sqrt{3}}{9\pi^3} \left[ \frac{\zeta_2}{2} + \ln(\aleph/k_F) \right], \quad (92)$$

and the terms  $E_{4,i}(\aleph)$  are given by subtracting from the respective integrands their values with the denominators replaced by those corresponding to  $\mathcal{I}_{1,2}^D$ . For example, the term  $E_{4,\text{II5}}(\aleph)$  is given by

$$E_{4,\text{II5}}(\aleph) = -\zeta(g-3) \sum_{\substack{\mathbf{i}, \mathbf{j}, \mathbf{k} \\ \mathbf{a}, \mathbf{c}}} n_{ijk} \times \left[ \frac{\bar{n}_{abcde}}{\mathcal{D}_{ab,ij} \mathcal{D}_{ce,ij} \mathcal{D}_{acd,ijk}} \Big|_{\substack{\mathbf{b}=\mathbf{i}+\mathbf{j}-\mathbf{a} \\ \mathbf{d}=\mathbf{i}+\mathbf{j}+\mathbf{k}-\mathbf{a}-\mathbf{c} \\ \mathbf{e}=\mathbf{i}+\mathbf{j}-\mathbf{c}}} - \frac{1}{\mathcal{D}_{ab}^{\aleph} \mathcal{D}_{ce}^{\aleph} \mathcal{D}_{acd}^{\aleph}} \Big|_{\substack{\mathbf{b}=-\mathbf{a} \\ \mathbf{d}=-\mathbf{a}-\mathbf{c} \\ \mathbf{e}=-\mathbf{c}}} \right], \quad (93)$$

with  $\mathcal{D}_{ab}^{\aleph} = \mathcal{D}_{ab} + \aleph^2/(k_F^2 M)$ . One finds

$$E_{4,\text{II5}}^{\text{MS}} = -\alpha(g-3) \times 0.0500(1), \quad (94)$$

$$E_{4,\text{IIA1}}^{\text{MS}} = -\alpha(3g-5) \times 0.0498(1), \quad (95)$$

$$E_{4,\text{II6}}^{\text{MS}} = \alpha(g-3) \times 0.0664(2), \quad (96)$$

$$E_{4,\text{III}(1+7+8)}^{\text{MS}} = \alpha(g-1) \times 0.0416(2). \quad (97)$$

The sums of the first two and the last two contributions are given by

$$E_{4,\text{II5}+\text{IIA1}}^{\text{MS}} = \alpha [0.00018(1) - (g-2) \times 0.1995(4)], \quad (98)$$

$$E_{4,\text{II6}+\text{III}(1+7+8)}^{\text{MS}} = \alpha [-0.0248(1) + (g-2) \times 0.1079(2)]. \quad (99)$$

From Eqs. (64) and (65), the relation between the ‘‘MS’’ values and the ‘‘R’’ ones is given by

$$E_{4,\text{II5}+\text{IIA1}}^{\text{MS}} = E_{4,\text{II5}+\text{IIA1}}^{\text{R}} - \alpha(g-2) \times 0.4581(8), \quad (100)$$

$$E_{4,\text{II6}+\text{III}(1+7+8)}^{\text{MS}} = E_{4,\text{II6}+\text{III}(1+7+8)}^{\text{R}} + \alpha(g-2) \times 0.1857(8). \quad (101)$$

As required, the difference between the ‘‘MS’’ values and the ‘‘R’’ values vanishes for  $g=2$ , see Sec. III.

<sup>8</sup> For II6 we separate again the power-divergent part II6(i), see Eq. (32).

## V. GROUND-STATE ENERGY AT FOURTH ORDER

Here, we summarize the results for the low-density expansion for the ground-state energy density  $E(k_F)$  of the dilute Fermi gas. The expansion reads

$$E(k_F) = n \varepsilon_F \left[ \frac{3}{5} + (g-1) \sum_{\nu=1}^{\infty} \mathcal{C}_{\nu}(k_F) \right], \quad (102)$$

with  $n = g k_F^3 / (6\pi^2)$  the fermion number density,  $\varepsilon_F = k_F^2 / (2M)$  the noninteracting Fermi energy, and  $g$  the spin multiplicity. The expansion coefficients up to fourth order are given by

$$\mathcal{C}_1(k_F) = \frac{2}{3\pi} k_F a_s, \quad (103)$$

$$\mathcal{C}_2(k_F) = \frac{4}{35\pi^2} (11 - 2 \ln 2) (k_F a_s)^2, \quad (104)$$

$$\mathcal{C}_3(k_F) = \left[ 0.0755732(0) + 0.0573879(0) (g-3) \right] (k_F a_s)^3 + \frac{1}{10\pi} (k_F a_s)^2 k_F r_s + \frac{1}{5\pi} \frac{g+1}{g-1} (k_F a_p)^3, \quad (105)$$

$$\mathcal{C}_4(k_F) = -0.0425(1) (k_F a_s)^4 + 0.0644872(0) (k_F a_s)^3 k_F r_s + \gamma_4(k_F) (g-2) (k_F a_s)^4. \quad (106)$$

The first two terms are the only ones for which closed-form expressions are known; these were first derived by Lenz [17] in 1929 and Lee and Yang [18] as well as de Dominicis and Martin [19] in 1957, respectively. The third-order term was first computed by de Dominicis and Martin [19] in 1957 for hard spheres with two isospin states, by Amusia and Efimov [21] in 1965 for a single species of hard spheres, and then by Efimov [23] in 1966 for the general dilute Fermi gas. It was also computed subsequently by various authors [11, 24–26, 47, 54, 57]. Initial studies of the fourth-order term for  $g = 2$  were performed by Baker in Refs. [22, 25, 52, 53], see also Ref. [28] for a discussion of these.

Up to third order, only two-body (i.e., ERE) parameters appear and the expansion is a polynomial in the Fermi momentum  $k_F$ . At higher orders  $N \geq 4$ , logarithmic terms  $\sim k_F^N \ln(k_F / \Lambda_0)$  enter, starting at  $N = 4$  for  $g > 2$ ; for  $g = 2$ , no logarithms emerge from  $S$ -wave interactions (as a consequence of the Pauli exclusion principle). The logarithms are accompanied by many-body couplings [at fourth order, the coupling  $D_0(\Lambda_0)$ ] whose dependence on the auxiliary scale  $\Lambda_0$  is such that the Fermi-momentum expansion is independent of  $\Lambda_0$ . The many-body couplings are renormalization scheme dependent and have to be matched to few-body (or many-body) observables calculated in the same scheme. Using a Galilean invariant regulator function and subtracting only divergent terms (“R” scheme), the  $g > 2$  part  $\gamma_4(k_F)$

Table I. Results for the contributions to the regular (i.e., non-logarithmic)  $a_s^4$  part of  $\mathcal{C}_4(k_F)$ . Diagrams with \* (\*\*) have UV power (logarithmic) divergences, which are subtracted by the respective counterterm contributions. Diagrams with \*\*\* have energy-denominator singularities. For the diagrams with logarithmic divergences, “(R)” denotes the result obtained using a regulator function and subtracting only divergent terms, and “(MS)” the result corresponding to DR with minimal subtraction. The uncertainty estimates take into account both the statistical Monte Carlo uncertainties and variations of the cutoff. The  $g$  factors are listed without the generic factor  $g(g-1)$ . See Fig. 3 for the diagrams.

diagram	$g$ factor	value
$\Pi^*$	1	+0.0383115(0)
$\text{I2}^* + \text{I3} + \text{I4}^* + \text{I5}^*$	1	+0.0148549(0)
I6	1	-0.0006851(0)
IA1	$g(g-3) + 4$	-0.003623(1)
IA2	$g(g-3) + 4$	-0.001672(1)
IA3	$g(g-3) + 4$	-0.003343(1)
$\text{II1}^* + \text{II2}^*$	$g-3$	+0.058359(1)
$\text{II3} + \text{II4}$	$g-3$	-0.003358(1)
$\text{II5}^{**}(\text{R})$	$g-3$	+0.0645(1)
$\text{II5}^{**}(\text{MS})$	$g-3$	-0.0500(1)
$\text{II6}^{***}(\text{R})$	$g-3$	-0.0265(2)
$\text{II6}^{***}(\text{MS})$	$g-3$	+0.0664(2)
$\text{II7} + \text{II12}$	$g-3$	+0.003923(1)
$\text{II8} + \text{II11}$	$g-3$	+0.007667(1)
II9	$g-3$	-0.000981(1)
II10	$g-3$	-0.000347(1)
$\text{IIA1}^{**}(\text{R})$	$3g-5$	+0.0647(1)
$\text{IIA1}^{**}(\text{MS})$	$3g-5$	-0.0498(1)
$\text{IIA2} + \text{IIA4}$	$3g-5$	+0.004122(1)
IIA3	$3g-5$	-0.000461(1)
IIA5	$3g-5$	+0.003542(1)
IIA6	$3g-5$	+0.003331(1)
$\text{III1}^{***,*}(\text{R}) + \text{III7} + \text{III8}^{***,*}$	$g-1$	-0.0513(2)
$\text{III1}^{***,*}(\text{MS}) + \text{III7} + \text{III8}^{***,*}$	$g-1$	+0.0416(2)
$\text{III2}^{***} + \text{III9} + \text{III10}^{***}$	$g-1$	+0.001650(1)
$(\text{II5} + \text{IIA1})_{g=2}$	1	+0.00018(1)
$(\text{II6} + \text{III1} + \text{III7} + \text{III8})_{g=2}^*$	1	-0.0248(1)
$\sum_{\text{diagrams}, g=2}$	1	-0.0425(1)

of the fourth-order term takes the form<sup>9</sup>

$$\gamma_4^{\text{R}}(k_F) = \frac{M D_0(\Lambda_0)}{108\pi^4 a_s^4} + 0.2707(4) - 0.00864(2) (g-2) + \frac{16}{27\pi^3} \left( 4\pi - 3\sqrt{3} \right) \ln(k_F / \Lambda_0). \quad (107)$$

On the other hand, using DR with minimal subtraction

<sup>9</sup> The logarithmic part of Eq. (107) was first derived by Efimov [20, 23] and subsequently in Refs. [10, 24, 26, 60]. Note that in the literature [10, 11, 20, 23, 24, 26, 45, 60] the arbitrary scale  $\Lambda_0$  is usually set to  $\Lambda_0 = 1/a_s$ .

(“MS” scheme) one obtains

$$\begin{aligned} \gamma_4^{\text{MS}}(k_F) &= \frac{MD_0^*(\Lambda_0)}{108\pi^4 a_s^4} - 0.0017(4) - 0.00864(2)(g-2) \\ &\quad + \frac{16}{27\pi^3} \left(4\pi - 3\sqrt{3}\right) \ln(k_F/\Lambda_0). \end{aligned} \quad (108)$$

The scaling of  $D_0(\Lambda_0)$  and  $D_0^*(\Lambda_0)$  with  $\Lambda_0$  is identical, and determined by the  $\Lambda_0$  independence of  $\gamma_4(k_F)$ . The values of  $D_0(\Lambda_0)$  and  $D_0^*(\Lambda_0)$  differ by a subtraction constant, i.e.,

$$D_0^*(\Lambda_0) = D_0(\Lambda_0) - \frac{108\pi^4 a_s^4}{M} \times 0.2724(8). \quad (109)$$

Although the subtraction constant is arbitrary, it is nevertheless pertinent to specify its value (i.e., to specify the renormalization scheme) in order to predict many-body results from few-body data, or vice versa.

The individual diagrammatic contributions to the  $C_0^4$  part of the fourth-order term are listed in Table I. The computations have been carried out using the Monte Carlo framework introduced in Ref. [61] to evaluate high-order many-body diagrams, see also Ref. [28]. The results for the contributions that involve logarithmic divergences, II5, II6, IIA1, and III(1+7+8), have the largest numerical uncertainties. For  $g = 2$ , slightly more precise results can be given for II5+IIA1 and II6+III(1+7+8), because then no logarithmic divergences occur (see Sec. III).

## VI. CONVERGENCE ANALYSIS AND RESUMMATIONS

As discussed above, for spin one-half fermions ( $g = 2$ ) the logarithmic terms from  $S$ -wave interactions cancel (by virtue of the Pauli principle). Logarithms still arise from  $P$ -wave interactions at higher orders, i.e., at a certain order  $N_{\text{log}}$ . The Fermi-momentum expansion for  $\mathcal{E} = E/E_0$ , truncated at an order  $N < N_{\text{log}}$ , is thus a polynomial in  $\delta = k_F a_s$ :

$$\mathcal{E}_N(\delta) = 1 + \sum_{\nu=1}^N \varepsilon_\nu \delta^\nu, \quad (110)$$

where  $E_0 = 3nk_F^2/(10M)$  is the energy density of the free Fermi gas, and the expansion coefficients  $\varepsilon_\nu \equiv \varepsilon_\nu(a_s, r_s, a_p, \dots)$  are completely determined by the ERE. In the following, we analyze the convergence behavior of Eq. (110) for two different cases. First, we examine the case where all ERE parameters beyond  $a_s$  are zero, which we denote by LO. Here, the coefficients in the  $k_F a_s$  expansion are given by

$$\begin{aligned} \{\varepsilon_\nu\} &= \left\{ \frac{10}{9\pi}, \frac{44 - 8 \ln 2}{21\pi^2}, \right. \\ &\quad \left. 0.0303089(0), -0.07076(39), \dots \right\}. \end{aligned} \quad (111)$$

Second, we consider the hard-sphere gas (HS) where  $a_s = 3r_s/2 = a_p$ , leading to

$$\{\varepsilon_\nu\} = \left\{ \frac{10}{9\pi}, \frac{44 - 8 \ln 2}{21\pi^2}, 0.383987(0), 0.00089(39), \dots \right\}. \quad (112)$$

In Sec. VIA we examine the convergence behavior of the LO and HS expansions and analyze the uncertainties of the predictions for  $E/E_0$ . We will find that in both cases the Fermi-momentum expansion is well-converged at fourth-order for  $|\delta| \lesssim 0.5$ . In Sec. VIB we then show that Padé and Borel resummations allow us to extend the domain of convergence to  $|\delta| \lesssim 1$ . Finally, in Sec. VIC we discuss the challenges regarding the calculation of the Fermi-momentum expansion beyond fourth order.

### A. Perturbative convergence and uncertainty estimates

In Ref. [28] we assessed the convergence pattern of the  $k_F a_s$  expansion at a given order  $N \leq 4$  by setting the next-higher coefficient  $\varepsilon_{N+1} = \pm \max[\varepsilon_{\nu \leq N}]$ . This spans an uncertainty band of width  $\Delta \mathcal{E}_N = 2|\varepsilon_{N+1}| \delta^{N+1}$ . Here, we use the pointwise Bayesian model with conjugate distributions developed in Refs. [62, 63] to estimate  $\varepsilon_{N+1}$  given the computed coefficients. This model allows one to evaluate posterior distributions analytically (given the conjugate prior) rather than through Monte Carlo sampling. Specifically, we treat the coefficients  $\varepsilon_\nu$  as random numbers drawn from a single normal distribution,<sup>10</sup>

$$\text{pr}(\varepsilon_\nu | \bar{c}^2) \stackrel{\text{i.i.d.}}{\sim} \frac{1}{\sqrt{2\pi\bar{c}^2}} \exp\left[-\frac{\varepsilon_\nu^2}{2\bar{c}^2}\right], \quad (113)$$

with mean zero and variance  $\bar{c}^2$ . The computed coefficients  $\varepsilon_{\nu \leq 4}$  are assumed to be known draws from this *a priori* unknown distribution function, while  $\varepsilon_{\nu > 4}$  are unknown. We also assume a scaled inverse- $\chi^2$  prior on  $\bar{c}^2$ ,

$$\text{pr}(\bar{c}^2) \sim \frac{(\tau_0^2 \eta_0/2)^{\eta_0/2}}{\Gamma(\eta_0/2)} \frac{\exp\left[-\frac{\eta_0 \tau_0^2}{2\bar{c}^2}\right]}{\bar{c}^{2(1+\eta_0/2)}}, \quad (114)$$

with  $\eta_0$  degrees of freedom and scale parameter  $\tau_0$ . By adjusting the hyperparameters we can incorporate our prior estimate of the (not computed) higher-order coefficients. We fix  $\eta_0 = 3$  and determine  $\tau_0^2$  by the requirement that the mean value  $\eta_0 \tau_0^2 / (\eta_0 - 2)$  equals  $|\max[\varepsilon_{\nu \leq N}]|$ . This prior choice disfavors high values for

<sup>10</sup>  $z \sim \dots$  is a common notation in statistics that reads “the variable  $z$  is distributed as  $\dots$ ”. The “i.i.d.” above the  $\sim$  indicates a set of independent and identically distributed (i.i.d.) random variables.



$\bar{c}^2$  and thus  $\varepsilon_{\nu > N}$ . Using Bayes' theorem and marginalizing over  $\bar{c}^2$ , one then finds that the posterior for a coefficient at order  $n > N$  is given by the Student's  $t$  distribution [62], i.e.,

$$\text{pr}(\varepsilon_{\nu > N} | \{\varepsilon_\nu\}_{\nu=1}^N, \tau^2) \sim t_\eta(\varepsilon_\nu; 0, \tau^2), \quad (115)$$

with

$$t_\eta(x; \mu, \tau^2) = \frac{1}{\sqrt{\pi\eta\tau^2}} \frac{\Gamma(\frac{\eta+1}{2})}{\Gamma(\frac{\eta}{2})} \left(1 + \frac{(x-\mu)^2}{\eta\tau^2}\right)^{-\frac{\eta+1}{2}}. \quad (116)$$

Here, the scale parameter  $\tau^2$  satisfies

$$\eta\tau^2 = \eta_0\tau_0^2 + \sum_{\nu=1}^N \varepsilon_\nu^2. \quad (117)$$

Furthermore,  $\eta = \eta_0 + n_c$ , where  $n_c$  is the number of coefficients in the set  $\{\varepsilon_\nu\}_{\nu=1}^{n_c}$  used to inform the probability distribution. We consider all available coefficients, i.e.,  $n_c = 4$ , so that all four known coefficients are used for each  $N \in \{1, 2, 3, 4\}$  in Eq. (115). Finally, from Bayes' theorem one then finds that the posterior distribution representing the uncertainty of  $\mathcal{E}_N(\delta)$  is given by [62]

$$\text{pr}(\mathcal{E}_N(\delta) | \{\varepsilon_\nu\}_{\nu=1}^N, \tau^2) \sim t_\eta(\mathcal{E}(\delta); \mathcal{E}_N(\delta), \delta^{2(N+1)}\tau^2), \quad (118)$$

where the variable  $\mathcal{E}(\delta)$  corresponds to the presumed exact results.

The convergence behavior of the Fermi-momentum expansion for the LO and the HS case is examined in Fig. 4. There, we show the perturbative results for  $\mathcal{E} = E/E_0$  obtained for truncation orders  $N = 2, 3, 4$  together with the respective 68% credibility intervals of our Bayesian analysis. Also shown are data points obtained from non-perturbative QMC computations [8, 64, 65]. One sees that the perturbative results are very close to the QMC data for  $|\delta| \lesssim 0.5$  but start to deviate strongly for  $|\delta| \gtrsim 1$ . In the LO case the relative error with respect to the QMC point at  $\delta = -0.5$  ( $\mathcal{E}_{\text{QMC}} \approx 0.862$ ) is 4.5% ( $\mathcal{E}_1 \approx 0.823$ ) at first, 0.8% ( $\mathcal{E}_2 \approx 0.870$ ) at second, 0.4% ( $\mathcal{E}_3 \approx 0.866$ ) at third, and 0.1% ( $\mathcal{E}_4 \approx 0.861$ ) at fourth order, while in the HS case the relative error at  $\delta = +0.5$  ( $\mathcal{E}_{\text{QMC}} \approx 1.254$ ) is 6.2% ( $\mathcal{E}_1 \approx 1.177$ ) at first, 2.5% ( $\mathcal{E}_2 \approx 1.223$ ) at second, 1.3% ( $\mathcal{E}_3 \approx 1.271$ ) at third, and 1.3% ( $\mathcal{E}_4 \approx 1.271$ ) at fourth order. The convergence of the expansion is slower in the HS case, which is signified by the relatively large size of the third-order coefficient there,  $\varepsilon_3 \approx 0.38$  (in the LO case it is  $\varepsilon_3 \approx 0.03$ ). The fourth-order HS coefficient  $\varepsilon_4 \approx 0.0009$  on the other hand is very small (due to a large cancellation between  $S$ - and  $P$ -wave contributions), so the third- and fourth-order HS curves in Fig. 4 are almost indistinguishable.

The Bayesian uncertainty bands in Fig. 4 are similar to those from the simple  $\varepsilon_{N+1} = \pm \max[\varepsilon_{\nu \leq N}]$  analysis, see Fig. 2 of Ref. [28]. In both schemes, going to higher orders

in the expansion reduces the width of the uncertainty bands for  $|\delta| \lesssim 1$ , and for  $|\delta| \lesssim 0.5$  the bands are very small for  $N = 4$ . This supports the conclusion that the expansion is well-converged at fourth order for  $|\delta| \lesssim 0.5$ , and diverges for  $|\delta| \gtrsim 1$ .<sup>11</sup> Note that these results do not depend on  $a_s$  being of natural size; only  $k_F a_s$  has to be small.

## B. Padé and Borel resummations

Resummation methods provide a means to extrapolate a (truncated) series beyond the region where well-converged results are obtained,  $|\delta| \lesssim 0.5$  in the present case. The two most common methods are Padé approximants [66, 67] and Borel resummation [68–71]. Below, we apply these two methods to the Fermi-momentum expansion for the LO case (with negative  $\delta$ ). We do not consider the HS case, because higher-order ERE parameters become relevant there at stronger coupling. Regarding Padé approximants, we restrict the discussion to those that give predictions for the Bertsch parameter  $\xi = \mathcal{E}(-\infty)$ .<sup>12</sup> In the Borel case we focus on the region of weak-to-intermediate coupling since only there (i.e., for  $|\delta| \lesssim 1$ ) the extrapolations are well converged.

### 1. Padé approximants

For a given formal power series

$$\mathcal{E}(\delta) = 1 + \sum_{\nu=1}^{\infty} \varepsilon_\nu \delta^\nu, \quad (119)$$

the Padé $[n, m]$  approximant is the rational function

$$\text{Padé}[n, m](\delta) = 1 + \frac{\sum_{k=1}^n a_k \delta^k}{1 + \sum_{l=1}^m b_l \delta^l}, \quad (120)$$

whose Maclaurin expansion matches the series up to order  $N = n + m$ . Only “diagonal” Padés with  $n = m$  have a nontrivial unitary limit, i.e.,  $\text{Padé}[n, n] \rightarrow 1 + a_n/b_n$  for  $\delta \rightarrow -\infty$ . To have meaningful results in the strong-coupling regime thus mandates the restriction to even  $N = 2n$ , i.e.,  $(N, n) = (2, 1)$  and  $(N, n) = (4, 2)$ .

The results obtained from the Padé $[1, 1]$  and  $[2, 2]$  approximants (which were already studied in Ref. [28]) are shown in the left panel of Fig. 4.<sup>13</sup> One sees that the

<sup>11</sup> More precisely, the Fermi-momentum expansion is an asymptotic series that diverges for  $N \rightarrow \infty$  for all  $|\delta| > 0$ , see Sec. II C. “Well-converged” means here that the result seems to be insensitive to lowering the truncation order.

<sup>12</sup> Padé predictions for the Bertsch parameter were previously studied by Baker [52, 53], see also Ref. [28].

<sup>13</sup> For a more extensive study of the Padé $[1, 1]$  approximant, see Ref. [72].

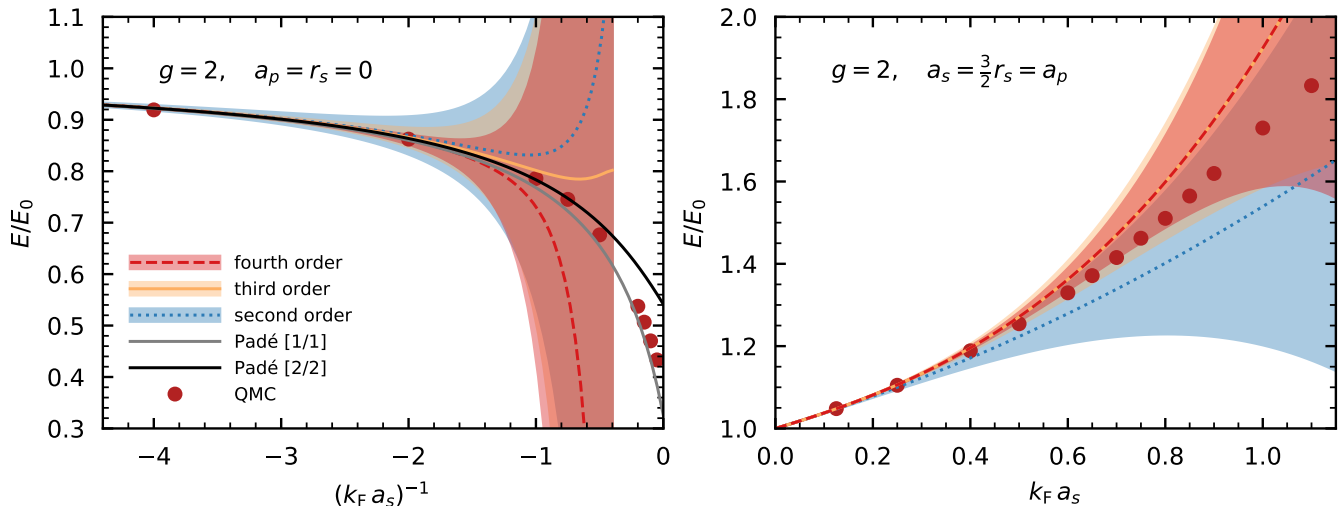


Figure 4. Convergence behavior of the Fermi-momentum expansion for the ground-state energy  $E/E_0$  of a dilute Fermi gas of spin one-half fermions with  $a_p = r_s = 0$  (LO, left panel) and  $a_s = 3r_s/2 = a_p$  (HS, right panel) at negative and positive  $k_F a_s$ , respectively. The respective uncertainty bands correspond to the 68% credibility intervals from our Bayesian estimation of the next-higher coefficient in the  $k_F a_s$  expansion. In the LO case we also show results obtained from two different Padé approximants, Padé[1, 1] (gray line) and Padé[2, 2] (black line). Finally, the thick red dots in each panel correspond to results from nonperturbative QMC computations [8, 64, 65]. Note that the  $x$ -axes in the two panels are different, and based on the available QMC data we show the attractive regime with  $a_s < 0$  in the left panel and the repulsive regime with  $a_s > 0$  in right panel. See the text for more details.

Padé[2, 2] approximant is very close to the QMC results for  $\delta \lesssim -1.2$ , while Padé[1, 1] is in better agreement close to the unitary limit  $\delta \rightarrow -\infty$ . Note however that pairing correlations become relevant for larger values of  $-\delta$ , and it is questionable that Padés can capture pairing effects (which are expected to be encoded in the high-order behavior of the  $k_F a_s$  expansion [39]) at low truncation orders. The range for the Bertsch parameter obtained from Padé[1, 1] and [2, 2],  $\xi_{\text{Padé}} \in [0.326, 0.541]$ , is consistent with the value  $\xi \approx 0.376$  extracted from experiments with cold atomic gases, and also with the extrapolated value for the normal (i.e., nonsuperfluid) Bertsch parameter  $\xi_n \approx 0.45$  [2]. Altogether, these results seem to indicate that Padé approximants converge in a larger region, compared to the Fermi-momentum expansion.

## 2. Borel resummation

Borel resummation is based on the Borel(-Leroy) transformed perturbation series, i.e.,

$$\mathcal{B}(t) \simeq 1 + \sum_{\nu=1}^{\infty} \frac{\varepsilon_{\nu}}{\Gamma(\nu+1+\beta_0)} t^{\nu}, \quad (121)$$

where the standard Borel transform corresponds to  $\beta_0 = 0$ . In contrast to the perturbative series [Eq. (119)], the Borel transformed series has a finite convergence radius: from the large-order behavior

$$\varepsilon_{\nu} \stackrel{\nu \rightarrow \infty}{\sim} a^{\nu} \Gamma(\nu+1+\beta), \quad (122)$$

one finds that the leading singularity of  $\mathcal{B}(t)$  is at  $t = 1/a$  [69, 73, 74]. Formally, in the so-called Borel-summable case where all singularities of  $\mathcal{B}(t)$  are off the positive real axis (in particular,  $a < 0$ ), the exact  $\mathcal{E}(\delta)$  is then obtained by first analytically continuing  $\mathcal{B}(t)$  beyond  $t = 1/|a|$  and then carrying out the inverse Borel transform:

$$\mathcal{E}(\delta) = \int_0^{\infty} dt e^{-t} t^{\beta_0} \mathcal{B}(t\delta). \quad (123)$$

Regarding practical applications where the perturbative series is only known up to a finite order  $N$ , this procedure allows one to construct approximants  $B_N(\delta)$  for  $\mathcal{E}(\delta)$  in terms of approximants  $\mathcal{B}_N(t)$  for  $\mathcal{B}(t)$ :

$$\mathcal{E}(\delta) \approx B_N(\delta) = \int_0^{\infty} dt e^{-t} t^{\beta_0} \mathcal{B}_N(t\delta). \quad (124)$$

A straightforward approach to construct  $\mathcal{B}_N(t)$  is the Padé-Borel method, which uses Padé approximants matched to the Borel series [Eq. (121)]. [We note that while the conjectured large-order behavior  $a = -1/\pi$  (and  $\beta = 0$ ) [39] would imply a non-Borel summable series for  $\delta < 0$ , we find that the Padé-Borel  $\mathcal{B}_N(t\delta)$  approximants for  $N \leq 4$  have no poles on the positive  $t$  axis for  $\delta < 0$ .]

In Fig. 5, we show the results for  $\mathcal{E}(\delta)$  from the second-, third-, and fourth-order Padé-Borel approximants obtained using the standard choice  $\beta_0 = 0$  for the Borel transform. Also shown are the corresponding perturbative results as well as the results from QMC computations from the left panel of Fig. 4. One sees that, compared to the perturbative results, the Borel approximants for  $\mathcal{E}(\delta)$

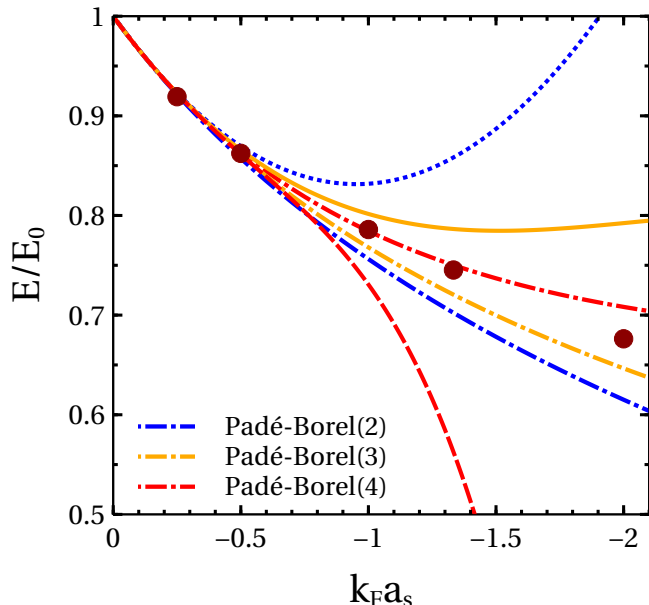


Figure 5. Results for the ground-state energy  $E/E_0$  of a dilute Fermi gas of spin one-half fermions with  $a_p = r_s = 0$  obtained from the Padé-Borel resummation method, see the text for details. The numbers in parentheses denote the underlying truncation order  $N$ . Also shown are results from QMC computations (filled red circles) as well as the perturbative results at second (dotted blue line), third (solid yellow line) and fourth order (dashed red line), see also Fig. 4.

have a much better convergence behavior for  $\delta > 0.5$ . Moreover, for  $|\delta| \lesssim 1$  the fourth-order Borel results are very close to the QMC data.

Overall, the results depicted in Figs. 4 and 5 show that Padé and Borel resummation methods allow to improve the convergence behavior of the  $C_0$  part of the Fermi-momentum expansion. To investigate this further would require future computations of higher-order series coefficients beyond fourth order. As discussed below, this however faces serious challenges.

### C. Beyond fourth order

The first complication regarding the calculation of coefficients beyond fourth order is the rapid increase of the number of Hugenholtz diagrams with  $N$ . Graph theory methods allow one to automatically generate diagrams [75–77], from which one finds that the number of diagrams without single-vertex loops increases as  $(1, 1, 3, 39, 840, 27300, \dots)$  for  $N = (1, 2, 3, 4, 5, 6, \dots)$ , where the number of the relevant normal diagrams increases as  $(1, 1, 3, 33, 668, 21572, \dots)$ .

For a given set of higher-order diagrams, the evaluation of those without UV divergences and those that have only simple ladder-type divergences (which are renormalized by two-body counterterms) would be relatively straightforward. That is, for a given diagram the only complica-

tion compared to a fourth-order diagram of similar type would be additional three-momentum integrals.

The main challenge concerning higher-order calculations lies (as in the fourth-order case) with UV divergences that are not renormalized by two-body counterterms. For instance, at fifth order one encounters several three-body scattering diagrams of the form of diagrams of Fig. 2 but with two additional intermediate states. These diagrams have logarithmic subdivergences that cancel if the diagrams are summed. The remaining linear UV divergence cancels for  $g = 2$  and is otherwise renormalized by a momentum-independent three-body counterterm. For the next diagonal Padé approximant (Padé[3, 3]) one would have to go to sixth order, where a much larger number of diagrams with complementary subdivergences and also the first momentum-dependent logarithmic divergence  $\sim Q^2 \ln(\Lambda/Q)$  appears in three-body scattering (see Sec. IID).

## VII. SUMMARY

In this paper we have discussed high-order perturbative EFT calculations for fermions at very low energy scales. In particular the issue of renormalization has been investigated in detail. We have then elaborated and expanded on our recent calculation [28] of the fourth-order term in the Fermi-momentum or  $k_F a_s$  expansion for the ground-state energy of the general dilute Fermi gas. The result for the complete (i.e., including both analytic and logarithmic terms) fourth-order coefficient has been given for two different regularization and renormalization schemes: cutoff regularization (with divergence subtraction) and dimensional regularization (with minimal subtraction).

The central results for the Fermi-momentum expansion are summarized in Sec. V, where in Table I the various contributions to the regular (i.e., nonlogarithmic)  $(k_F a_s)^4$  part of the fourth-order term are listed. In Sec. VI we have then investigated the convergence behavior of the expansion for the case of spin one-half fermions. Using Bayesian methods and comparing against results from nonperturbative QMC computations, we found that the expansion is well-converged at fourth order for  $|k_F a_s| \lesssim 0.5$ , and exhibits divergent behavior for  $|k_F a_s| \gtrsim 1$ , see Fig. 4. (To be precise, the  $k_F a_s$  expansion is a divergent asymptotic series; by “divergent behavior” we mean that the accuracy of the result at low truncation orders is deficient.)

Furthermore, we have shown that Padé-Borel resummations (of the  $a_s$ -only part of the expansion) improve the convergence and give well-converged results at fourth order in the region  $|k_F a_s| \lesssim 1$ , see Fig. 5. Accurate results throughout the entire BCS regime with negative  $k_F a_s$  (and into the BEC region) can however be obtained via resummations that incorporate constraints on the behavior for  $k_F a_s \rightarrow -\infty$  from QMC computations [78, 79]. Given the technical challenges that arise beyond fourth

order, it is unlikely that the  $k_F a_s$  expansion will be evaluated to even higher precision in the near future.

Our results for the Fermi-momentum expansion at fourth order provide important constraints for ultracold atoms and dilute neutron matter. Specifically, our results serve as useful benchmarks for future QMC simulations of dilute Fermi systems and may be used to construct improved models of neutron -star crusts. Future work may be targeted at high-order calculations of the dilute Fermi gas expansion at finite temperature.

## ACKNOWLEDGMENTS

We thank T. Duguet, H.-W. Hammer, J.A. Melendez, and S. Wesolowski for useful discussions, and P. Arthuis

for sending us his list of fifth- and sixth-order diagrams. We are also grateful to S. Gandolfi and S. Pilati for sending us their QMC results. This work is supported in part by the Deutsche Forschungsgemeinschaft (DFG, German Research Foundation) – Project-ID 279384907 – SFB 1245, the US Department of Energy, the Office of Science, the Office of Nuclear Physics, and SciDAC under awards DE-SC00046548 and DE-AC02-05CH11231. C.D. acknowledges support by the Alexander von Humboldt Foundation through a Feodor-Lynen Fellowship. This material is based upon work supported by the U.S. Department of Energy, Office of Science, Office of Nuclear Physics, under the FRIB Theory Alliance award DE-SC0013617. Computational resources have been provided by the Lichtenberg high performance computer of the TU Darmstadt.

- 
- [1] E. Braaten and H.-W. Hammer, *Phys. Rep.* **428**, 259 (2006).
  - [2] M. J. H. Ku, A. T. Sommer, L. W. Cheuk, and M. W. Zwierlein, *Science* **335**, 563 (2012).
  - [3] N. Navon, S. Nascimbène, F. Chevy, and C. Salomon, *Science* **328**, 729 (2010).
  - [4] I. Bloch, J. Dalibard, and W. Zwerger, *Rev. Mod. Phys.* **80**, 885 (2008).
  - [5] S. Giorgini, L. P. Pitaevskii, and S. Stringari, *Rev. Mod. Phys.* **80**, 1215 (2008).
  - [6] C. Chin, R. Grimm, P. Julienne, and E. Tiesinga, *Rev. Mod. Phys.* **82**, 1225 (2010).
  - [7] J. Carlson, S. Gandolfi, K. E. Schmidt, and S. Zhang, *Phys. Rev. A* **84**, 061602 (2011).
  - [8] S. Gandolfi, A. Gezerlis, and J. Carlson, *Ann. Rev. Nucl. Part. Sci.* **65**, 303 (2015).
  - [9] J. Polchinski, *Nucl. Phys. B* **231**, 269 (1984).
  - [10] E. Braaten and A. Nieto, *Phys. Rev. B* **55**, 8090 (1997).
  - [11] H.-W. Hammer and R. J. Furnstahl, *Nucl. Phys. A* **678**, 277 (2000).
  - [12] S. K. Bogner, R. J. Furnstahl, and A. Schwenk, *Prog. Part. Nucl. Phys.* **65**, 94 (2010).
  - [13] J. W. Holt, N. Kaiser, and W. Weise, *Prog. Part. Nucl. Phys.* **73**, 35 (2013).
  - [14] K. Hebeler, J. D. Holt, J. Menéndez, and A. Schwenk, *Ann. Rev. Nucl. Part. Sci.* **65**, 457 (2015).
  - [15] C. Drischler, W. Haxton, K. McElvain, E. Mereghetti, A. Nicholson, P. Vranas, and A. Walker-Loud, *Prog. Part. Nucl. Phys.* , 103888 (2021), arXiv:1910.07961.
  - [16] C. Drischler, J. W. Holt, and C. Wellenhofer, *Annu. Rev. of Nucl. Part. Sci.* **71**, 403 (2021), arXiv:2101.01709.
  - [17] W. Lenz, *Z. Phys.* **56**, 778 (1929).
  - [18] T. D. Lee and C. N. Yang, *Phys. Rev.* **105**, 1119 (1957).
  - [19] C. de Dominicis and P. C. Martin, *Phys. Rev.* **105**, 1417 (1957).
  - [20] V. N. Efimov, *Phys. Lett.* **15**, 49 (1965).
  - [21] M. Y. Amusia and V. N. Efimov, *Sov. Phys. JETP* **20**, 388 (1965).
  - [22] G. A. Baker, *Phys. Rev.* **140**, 9 (1965).
  - [23] V. N. Efimov, *Sov. Phys. JETP* **22**, 135 (1966).
  - [24] M. Y. Amusia and V. N. Efimov, *Ann. Phys.* **47**, 377 (1968).
  - [25] G. A. Baker, *Rev. Mod. Phys.* **43**, 479 (1971).
  - [26] R. F. Bishop, *Ann. Phys.* **77**, 106 (1973).
  - [27] E. H. Lieb, R. Seiringer, and J. P. Solovej, *Phys. Rev. A* **71**, 053605 (2005).
  - [28] C. Wellenhofer, C. Drischler, and A. Schwenk, *Phys. Lett. B* **802**, 135247 (2020).
  - [29] D. B. Kaplan, M. J. Savage, and M. B. Wise, *Nucl. Phys. B* **534**, 329 (1998).
  - [30] J. V. Steele, arXiv:nucl-th/0010066v2.
  - [31] R. J. Furnstahl, H.-W. Hammer, and N. Tiffessa, *Nucl. Phys. A* **689**, 846 (2001).
  - [32] R. J. Furnstahl and H.-W. Hammer, *Phys. Lett. B* **531**, 203 (2002).
  - [33] T. Schäfer, C.-W. Kao, and S. R. Cotanch, *Nucl. Phys. A* **762**, 82 (2005).
  - [34] L. Contessi, A. Lovato, F. Pederiva, A. Roggero, J. Kirscher, and U. van Kolck, *Phys. Lett. B* **772**, 839 (2017).
  - [35] A. Bansal, S. Binder, A. Ekström, G. Hagen, G. R. Jansen, and T. Papenbrock, *Phys. Rev. C* **98**, 054301 (2018).
  - [36] J. C. Collins, *Renormalization*, Cambridge Monographs on Mathematical Physics, Vol. 26 (Cambridge University Press, Cambridge, 1986).
  - [37] M. Drissi, T. Duguet, and V. Somà, *Eur. Phys. J. A* **56**, 119 (2020).
  - [38] U. van Kolck, *Nucl. Phys. A* **645**, 273 (1999).
  - [39] M. Mariño and T. Reis, *J. Stat. Mech.* **2019**, 123102 (2019).
  - [40] J. Feldman, M. Salmhofer, and E. Trubowitz, *J. Stat. Phys.* **84**, 1209 (1996).
  - [41] V. Rivasseau, *From Perturbative to Constructive Renormalization* (Princeton University Press, Princeton, 1991).
  - [42] R. Rossi, T. Ohgoe, K. Van Houcke, and F. Werner, *Phys. Rev. Lett.* **121**, 130405 (2018).
  - [43] P. F. Bedaque, H. Hammer, and U. van Kolck, *Nucl. Phys. A* **646**, 444 (1999).
  - [44] P. F. Bedaque, H.-W. Hammer, and U. van Kolck, *Phys. Rev. Lett.* **82**, 463 (1999).
  - [45] E. Braaten, H.-W. Hammer, and T. Mehen, *Phys. Rev. Lett.* **88**, 040401 (2002).
  - [46] H.-W. Hammer, S. König, and U. van Kolck, *Rev. Mod.*

- Phys. **92**, 025004 (2020).
- [47] N. Kaiser, *Nucl. Phys. A* **860**, 41 (2011).
- [48] R. J. Furnstahl and H.-W. Hammer, *Ann. Phys.* **302**, 206 (2002).
- [49] Y. Nishida and D. T. Son, *Phys. Rev. Lett.* **97**, 050403 (2006).
- [50] R. Haussmann, W. Rantner, S. Cerrito, and W. Zwerger, *Phys. Rev. A* **75**, 023610 (2007).
- [51] H. Tajima, P. van Wyk, R. Hanai, D. Kagamihara, D. Inotani, M. Horikoshi, and Y. Ohashi, *Phys. Rev. A* **95**, 043625 (2017).
- [52] G. A. Baker, *Phys. Rev. C* **60**, 054311 (1999).
- [53] G. A. Baker, *Int. J. Mod. Phys. B* **15**, 1314 (2001).
- [54] N. Kaiser, *Eur. Phys. J. A* **48**, 148 (2012).
- [55] C. Wellenhofer, *Phys. Rev. C* **99**, 065811 (2019).
- [56] W. Kohn and J. M. Luttinger, *Phys. Rev.* **118**, 41 (1960).
- [57] N. Kaiser, *Eur. Phys. J. A* **53**, 104 (2017).
- [58] N. Muskhelishvili, *Singular Integral Equations* (Dover Publications, New York, 2008).
- [59] A. Szabo and N. S. Ostlund, *Modern Quantum Chemistry* (Dover Publications, New York, 1982).
- [60] E. Braaten and A. Nieto, *Eur. Phys. J. B* **11**, 143 (1999).
- [61] C. Drischler, K. Hebeler, and A. Schwenk, *Phys. Rev. Lett.* **122**, 042501 (2019).
- [62] J. A. Melendez, R. J. Furnstahl, D. R. Phillips, M. T. Pratola, and S. Wesolowski, *Phys. Rev. C* **100**, 044001 (2019).
- [63] J. A. Melendez, S. Wesolowski, and R. J. Furnstahl, *Phys. Rev. C* **96**, 024003 (2017).
- [64] S. Gandolfi, private communication (2018).
- [65] S. Pilati, G. Bertaina, S. Giorgini, and M. Troyer, *Phys. Rev. Lett.* **105**, 030405 (2010).
- [66] G. A. Baker and P. Graves-Morris, *Padé Approximants* (Cambridge University Press, Cambridge, 1996).
- [67] C. M. Bender and S. A. Orszag, *Advanced Mathematical Methods for Scientists and Engineers I: Asymptotic Methods and Perturbation Theory* (Springer, Berlin, 1999).
- [68] J. Zinn-Justin, *Phys. Rep.* **70**, 109 (1981).
- [69] H. Kleinert and V. Schulte-Frohlinde, *Critical properties of  $\phi^4$ -theories* (World Scientific, River Edge, 2001).
- [70] D. Dorigoni, *Ann. Phys.* **409**, 167914 (2019).
- [71] I. Aniceto, G. Başar, and R. Schiappa, *Phys. Rep.* **809**, 1 (2019).
- [72] A. Boulet and D. Lacroix, *J. Phys. G* **46**, 105104 (2019).
- [73] O. Costin and G. V. Dunne, *J. Phys. A* **52**, 445205 (2019).
- [74] I. Caprini, *Phys. Rev. D* **100**, 056019 (2019).
- [75] P. D. Stevenson, *Int. J. Mod. Phys. C* **14**, 1135 (2003).
- [76] P. Arthuis, T. Duguet, A. Tichai, R.-D. Lasserri, and J.-P. Ebran, *Comp. Phys. Comm.* **240**, 202 (2019).
- [77] P. Arthuis, A. Tichai, J. Ripoché, and T. Duguet, *Comp. Phys. Comm.* **261**, 107677 (2021).
- [78] C. Wellenhofer, D. R. Phillips, and A. Schwenk, *Phys. Rev. Res.* **2**, 043372 (2020).
- [79] C. Wellenhofer, D. R. Phillips, and A. Schwenk, *Phys. Status Solidi B* **2**, 2000554 (2021).